Integrated Computational Materials and Process Engineering

An Overview of Research Projects at the IBF

Sebastian Münstermann

The IBF in Figures

Institute of Metal Forming

Chair of Forming Technologies
Dr. Bailly (interim) → Prof. Junhe Lian

Chair of Material Modelling in Forming Technology
Prof. Münstermann

THIRD-PARTY FUNDS 2022
SUM OF BOTH CHAIRS: 5,3 MIO. €

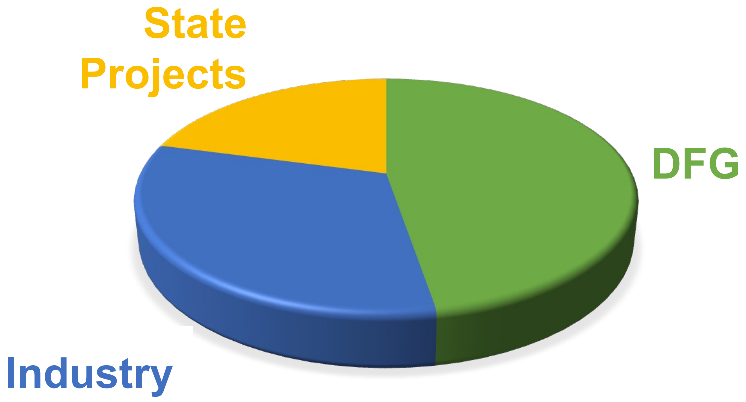

STAFF 2023
SUM OF BOTH CHAIRS: 126 EMPLOYEES

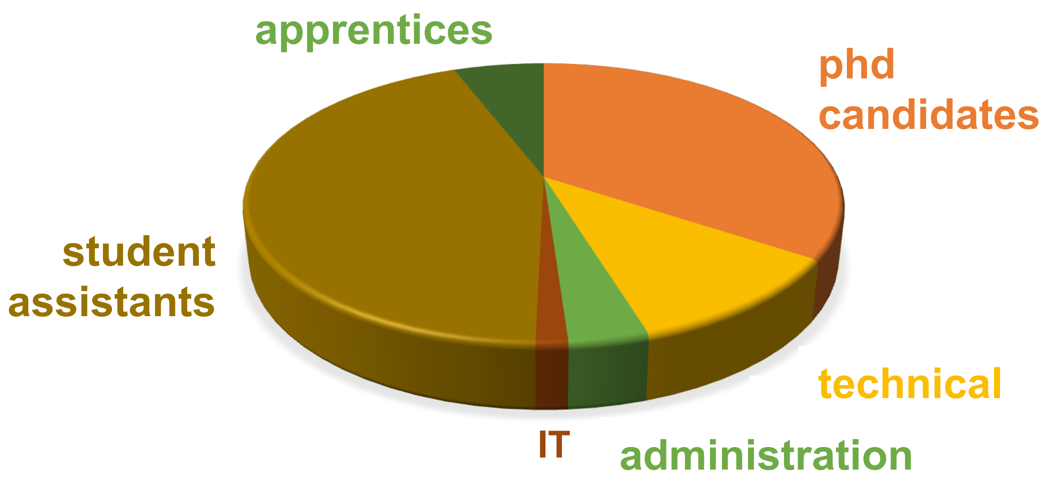

Research at the IBF - Materials, Processes and Application

Process Chains of Sheet and Bulk Metal Forming

Material	Semi-finished	Shaped Parts	Products
Steel	Strip Casting	Forging	Material
Non-Ferrous	Hot Rolling	Ring Rolling	Aerospace
Aluminum	Cold Rolling	Stretch Forming	Automotive
Nickel-Based	High-Precision Rolling	ISF	Construction
Titanium	Roll Bonding	Deep Drawing	E-Mobility
Copper	…	Hot-Gas Forming	Energy
…		…	Medical

Research at the IBF – Digitalization

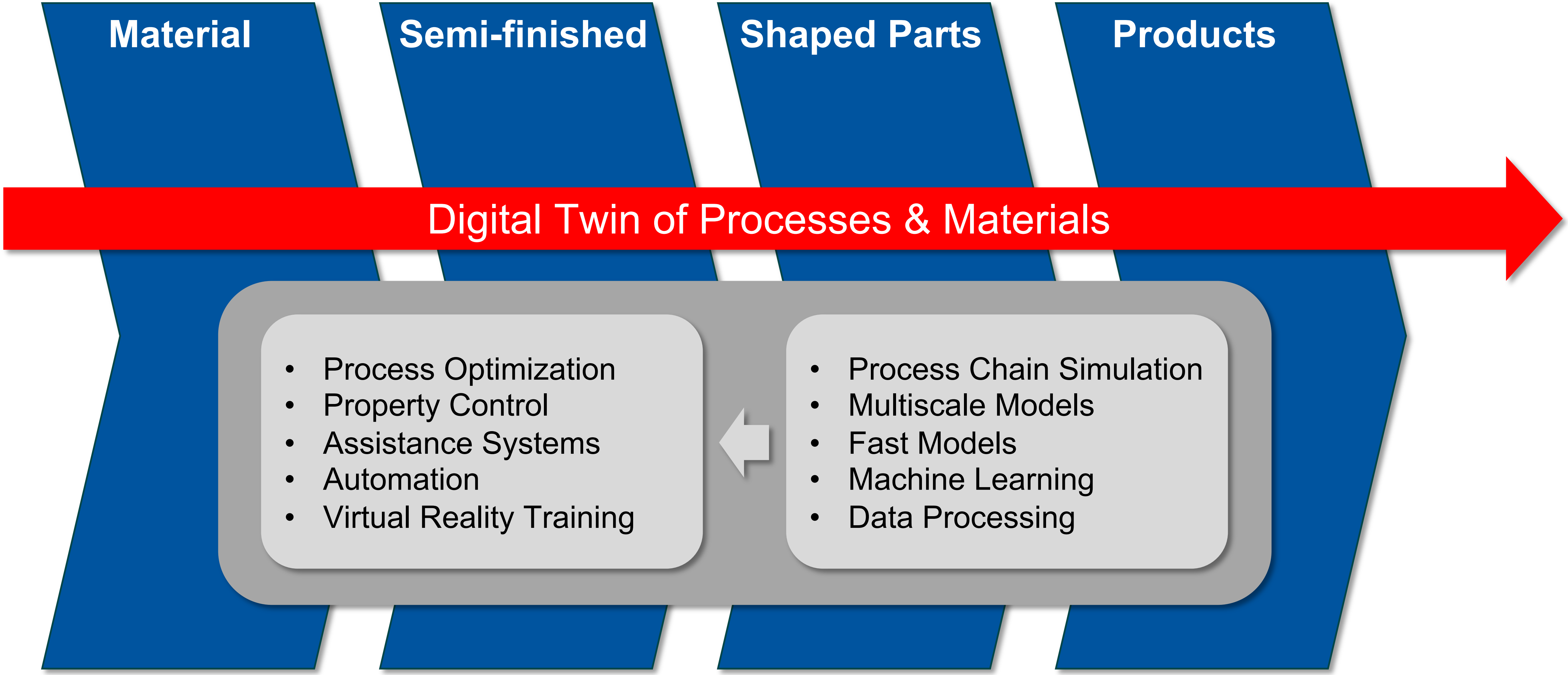

Research at the IBF – Sustainability

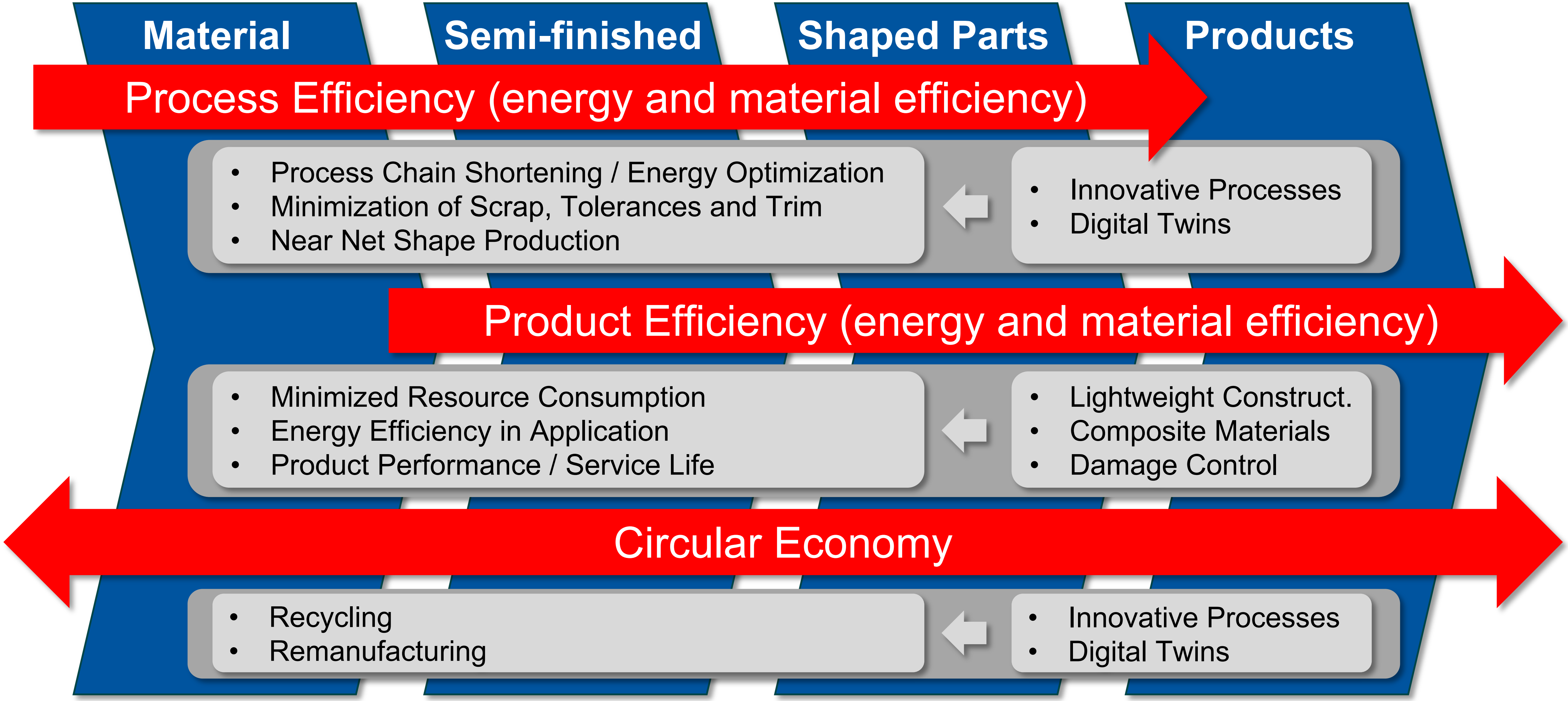

Integrated Computational Materials (and Process) Engineering

Motivation and Method

The material´s manufacturing process defines its microstructure!

Significant influence of the microstructure on the properties of the material!

Processing semi-finished product leads to microstructure & property modification!

Microstructure affects effective properties as well as component performance!

RVE simulations can connect microstructure, properties and performance

Integrated Computational Materials (and Process) Engineering

Challenges

process

casting | rolling | annealing | component forming | welding | service

microstructure

grain size, grain shape, crystallographic texture, dislocation density, precipitates, …

properties

strength, toughness, fatigue resistance, corrosion resistance, …

performance

evolution of load carrying capacity and expected lifetime

Holistic view on the process chain

Interaction of different loading steps must be considered – including the component use

1. Manufacturing step

2. Manufacturing step

Static component use

Cyclic component use

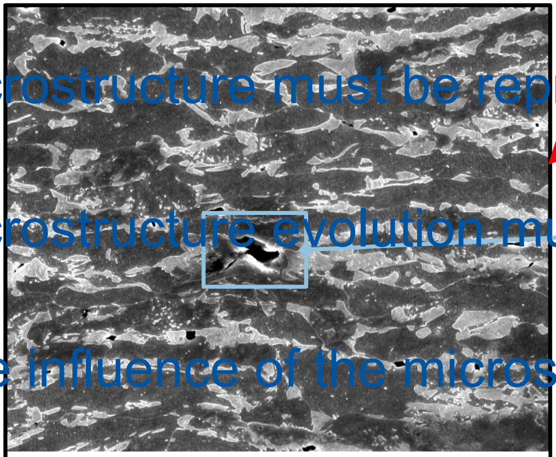

Pores from the forming process are critical for fatigue strength!

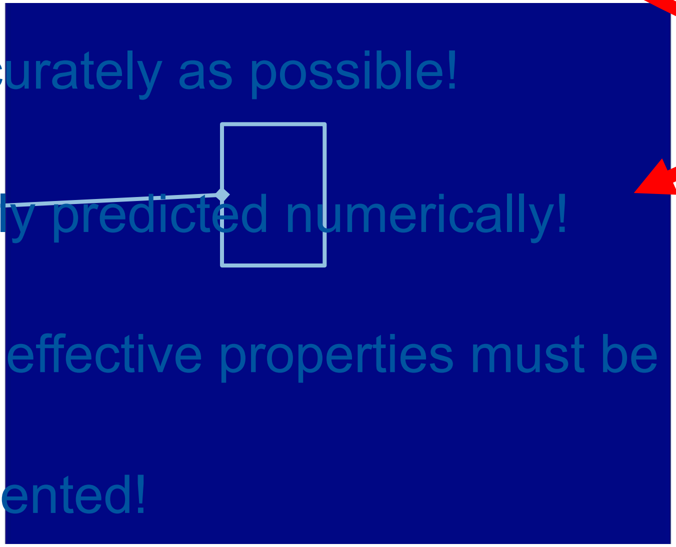

Microstructure must be reproduced as accurately as possible!

Microstructure evolution must be accurately predicted numerically!

The influence of the microstructure on the effective properties must be predicted!

Interaction of mechanisms must be represented!

RVE Generation

Microstructure must be reproduced as accurately as possible!

Microstructure evolution must be accurately predicted numerically!

The influence of the microstructure on the effective properties must be predicted!

Interaction of mechanisms must be represented!

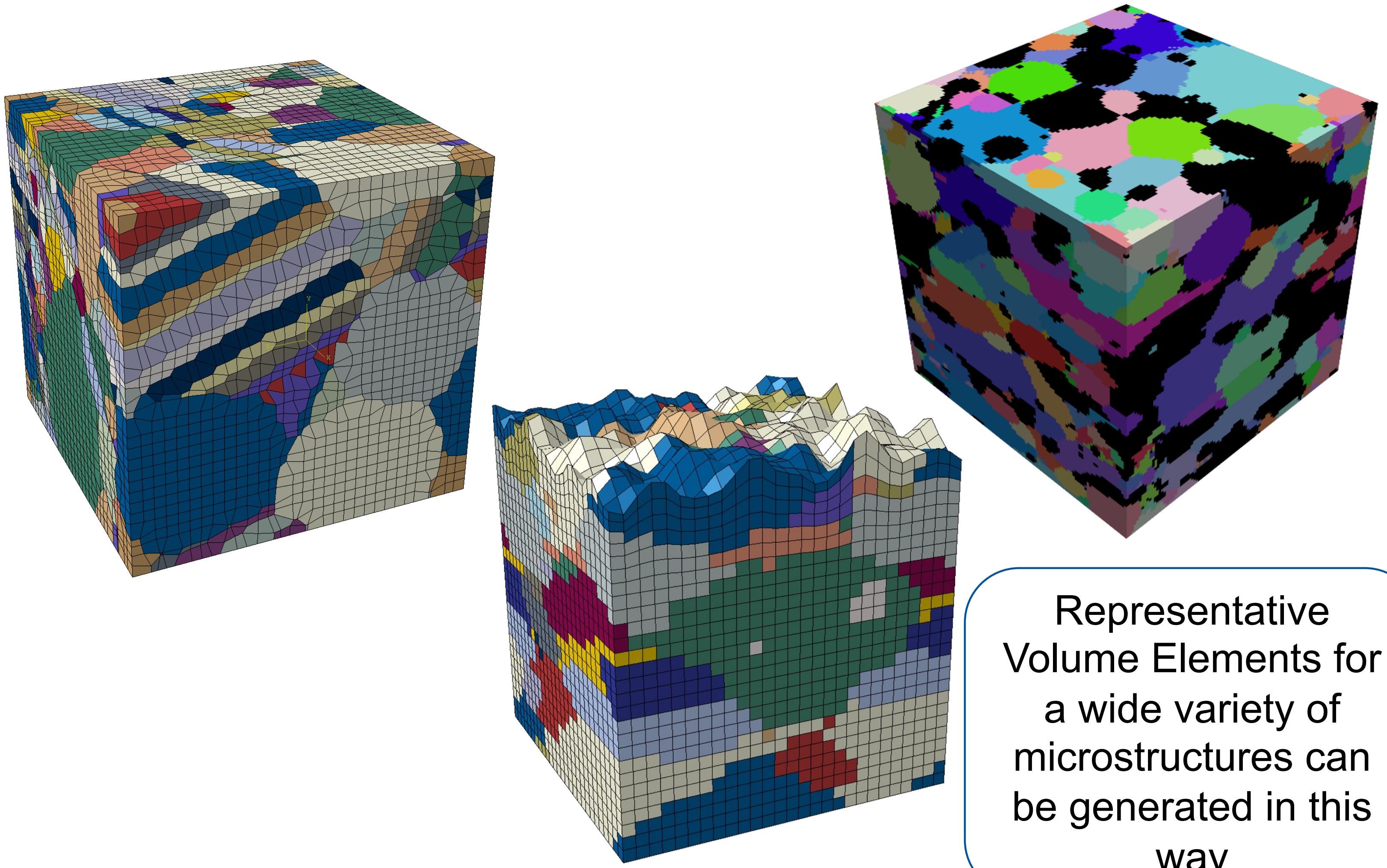

Representative Volume Elements for a wide variety of microstructures can be generated in this way

RVE Generation

Microstructure must be reproduced as accurately as possible!

Microstructure evolution must be accurately predicted numerically!

The influence of the microstructure on the effective properties must be predicted!

Interaction of mechanisms must be represented!

RVE-Simulation

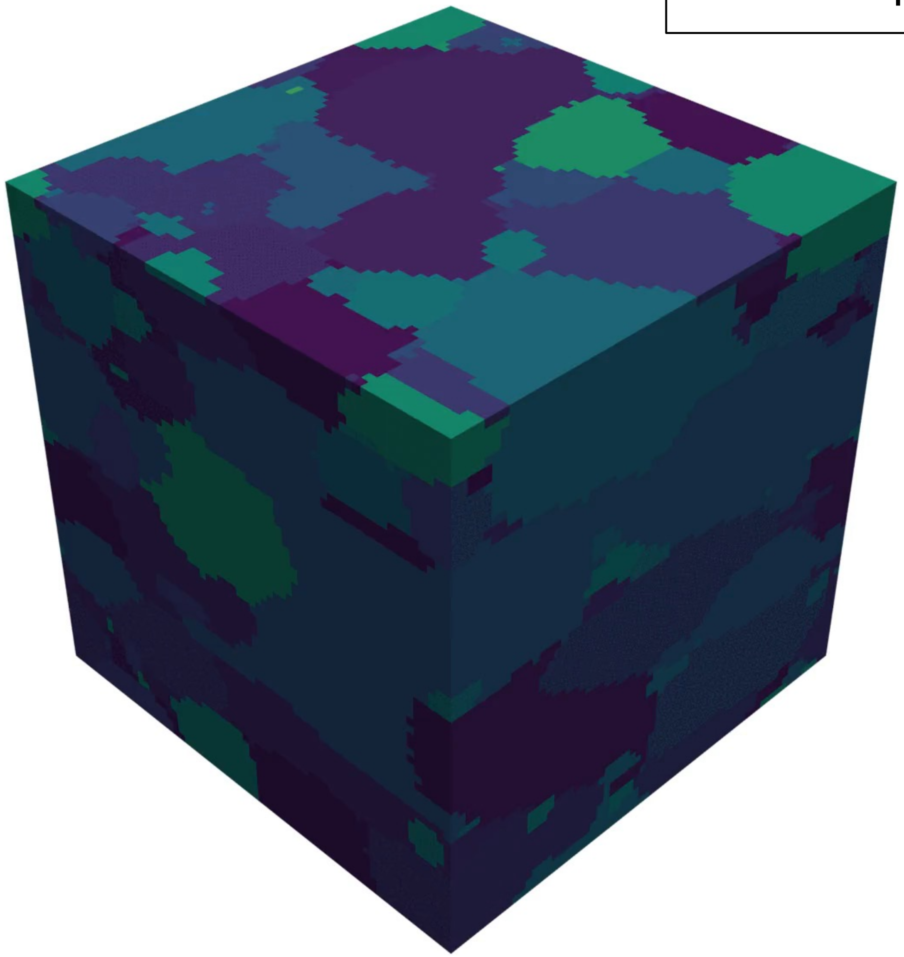

Modelling the microstructure evolution during processing

Microstructure must be reproduced as accurately as possible!

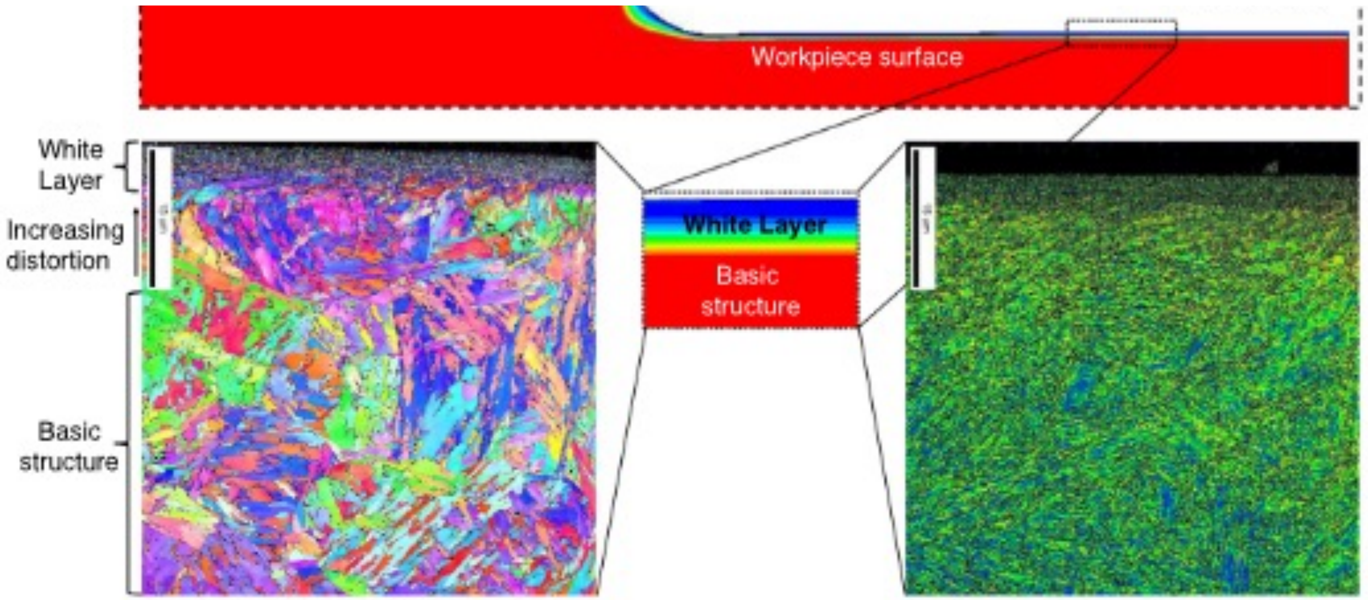

Microstructure evolution must be accurately predicted numerically!

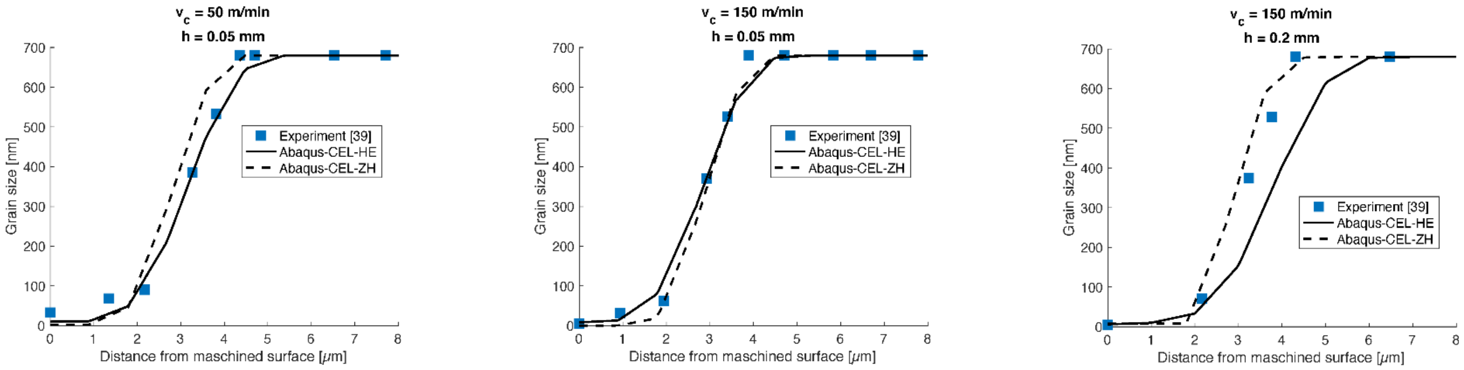

The influence of the microstructure on the effective properties must be predicted!

Interaction of mechanisms must be represented!

Modelling the microstructure evolution during processing

Microstructure must be reproduced as accurately as possible!

Microstructure evolution must be accurately predicted numerically!

The influence of the microstructure on the effective properties must be predicted!

Interaction of mechanisms must be represented!

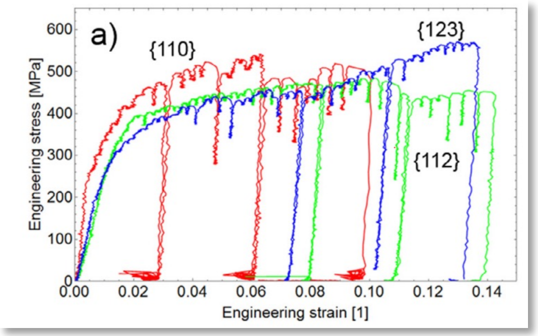

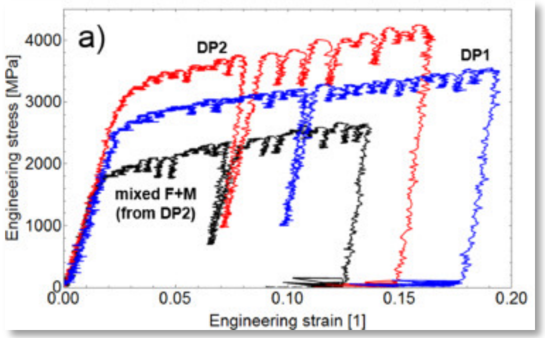

Individual crystal plasticity parameters are transferred to an RVE...

Slip rate

$$\dot{\gamma}^\alpha = \dot{\gamma}_0 \left| \frac{\tau^\alpha - \chi^\alpha}{\tau_c^\alpha} \right|^a sgn(\tau^\alpha - \chi^\alpha)$$

Backstress evolution law

$$\dot{\chi}^\alpha = A\dot{\gamma}^\alpha - B|\dot{\gamma}^\alpha|\chi^\alpha$$

Resolved shear stress

$$\tau^\alpha = \boldsymbol{\sigma}[m^\alpha \otimes n^\alpha]$$

Critical resolved shear stress

$$\tau_c^\alpha = \tau_i + q^{\alpha\beta}\left[h_0\left(1 - \frac{\tau_c^\beta}{\tau_s}\right)^b\right]|\Delta\gamma^\beta|$$

Initial critical resolved shear stress

$$\tau^i = \tau_{av} + \frac{k}{\sqrt{d}}$$

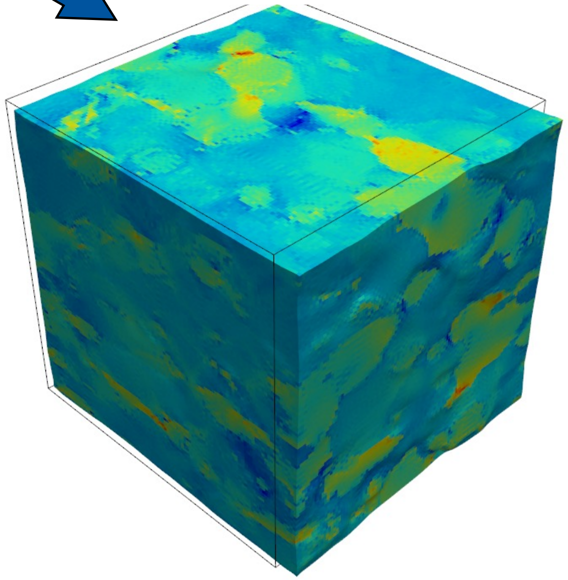

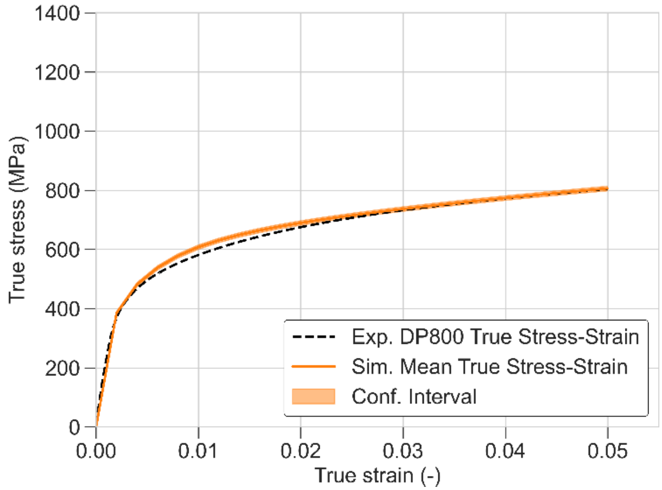

Modelling the microstructure evolution during processing

Microstructure must be reproduced as accurately as possible!

Microstructure evolution must be accurately predicted numerically!

The influence of the microstructure on the effective properties must be predicted!

Interaction of mechanisms must be represented!

Experimentally characterized surface roughness after forward extrusion

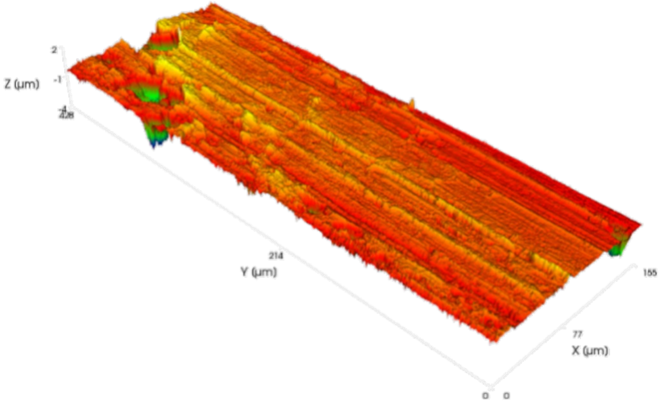

Macro-Micro transfer

sRVE sith surface rouhness

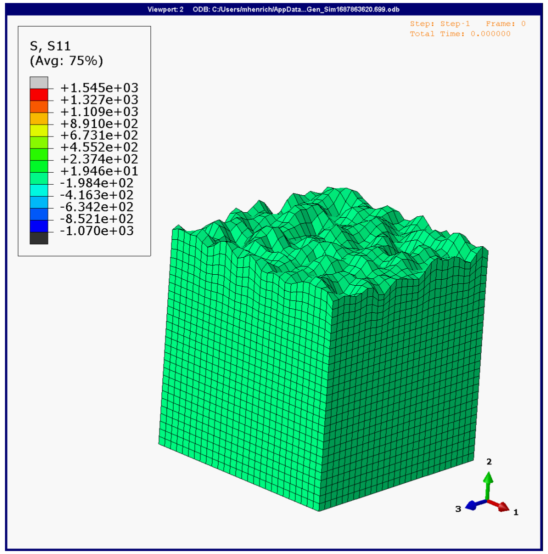

How can we predict fatigue lifetimes in RVE simulations?

Example 1: Microstructure sensitive fatigue modelling

How does the microstructure affect the fatigue resistance?

Effect of inclusions on accumulated plastic strain

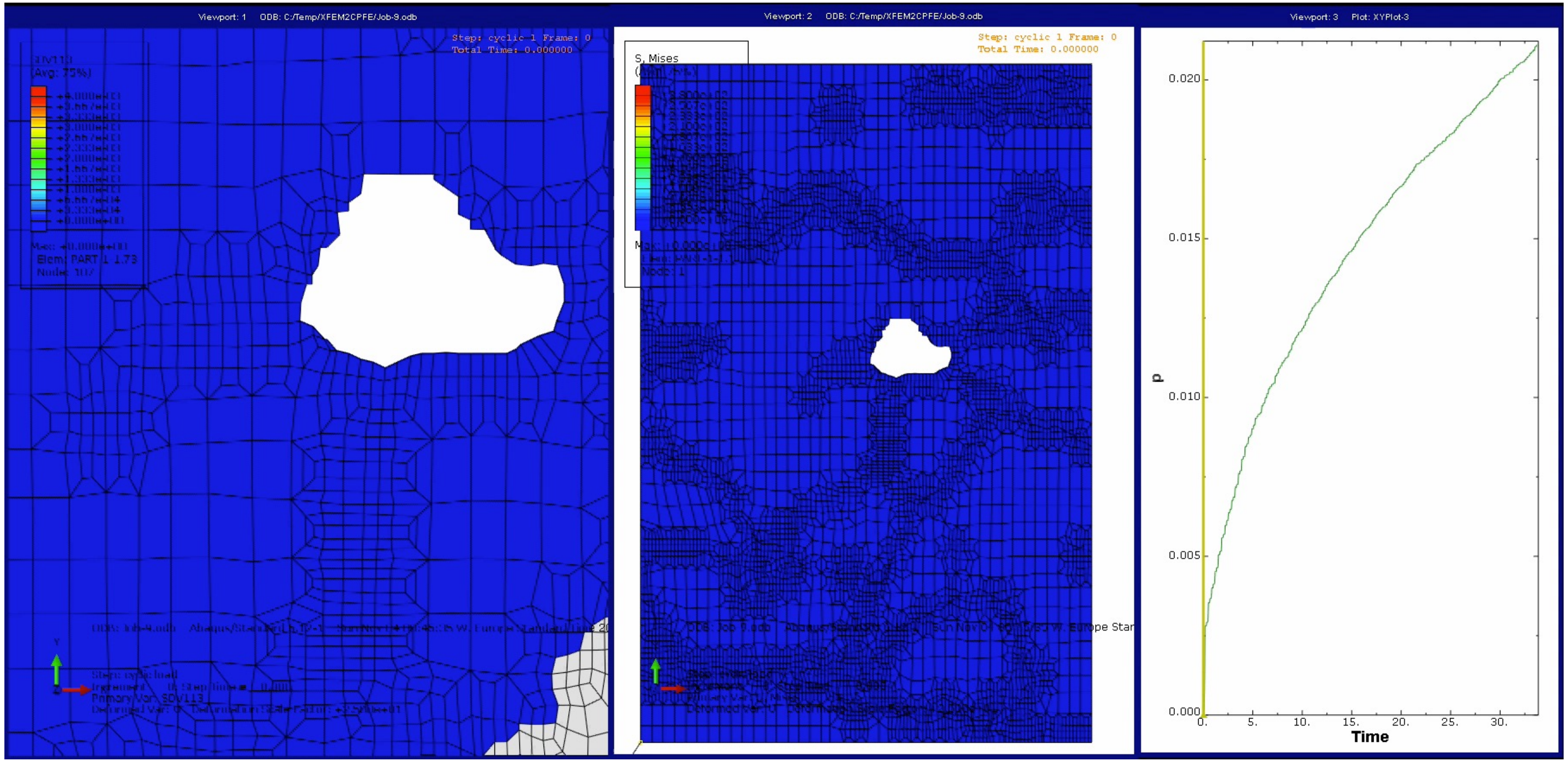

Selection of RVEs of the simulation set

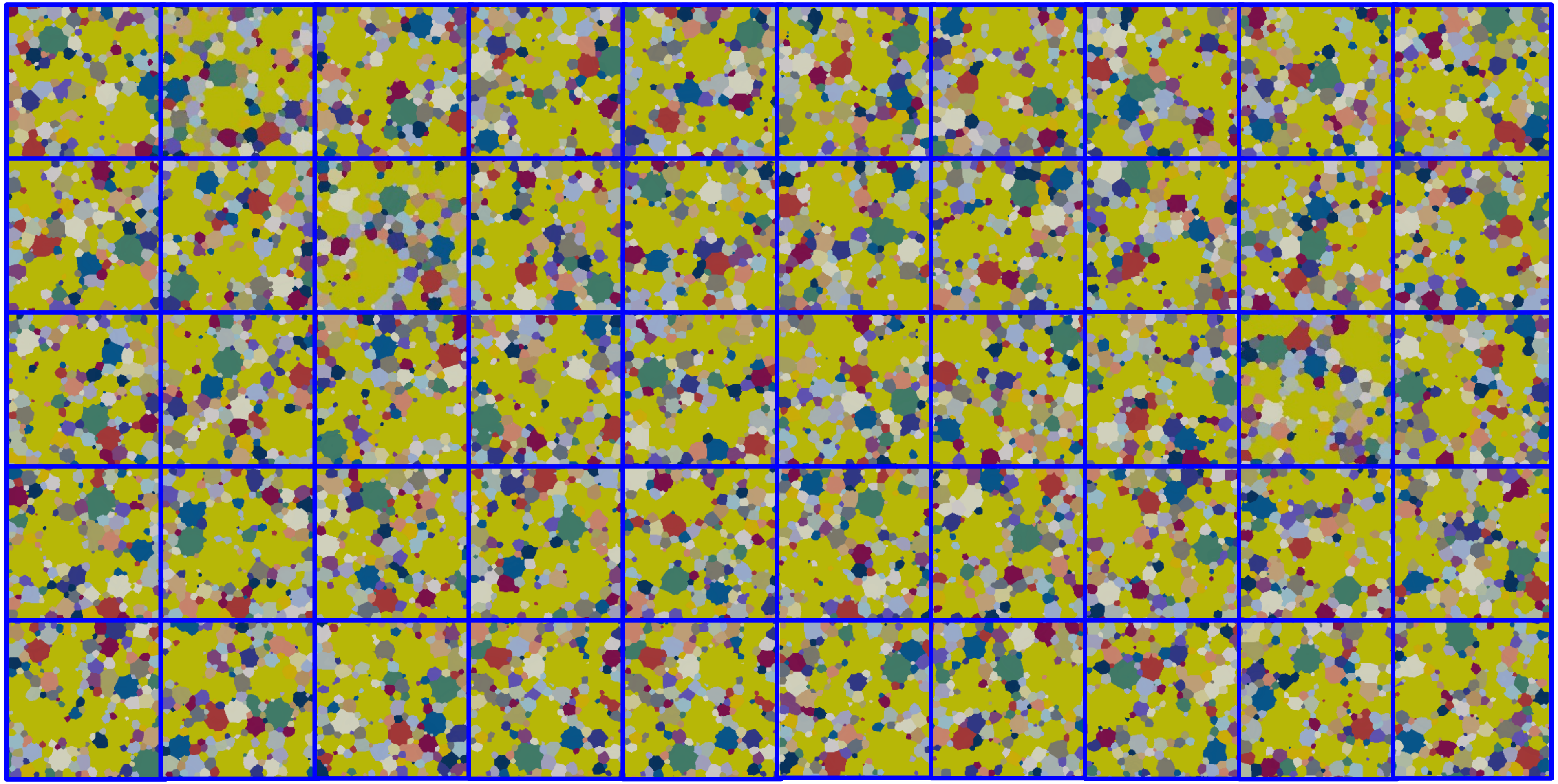

Response of RVEs of the simulation set

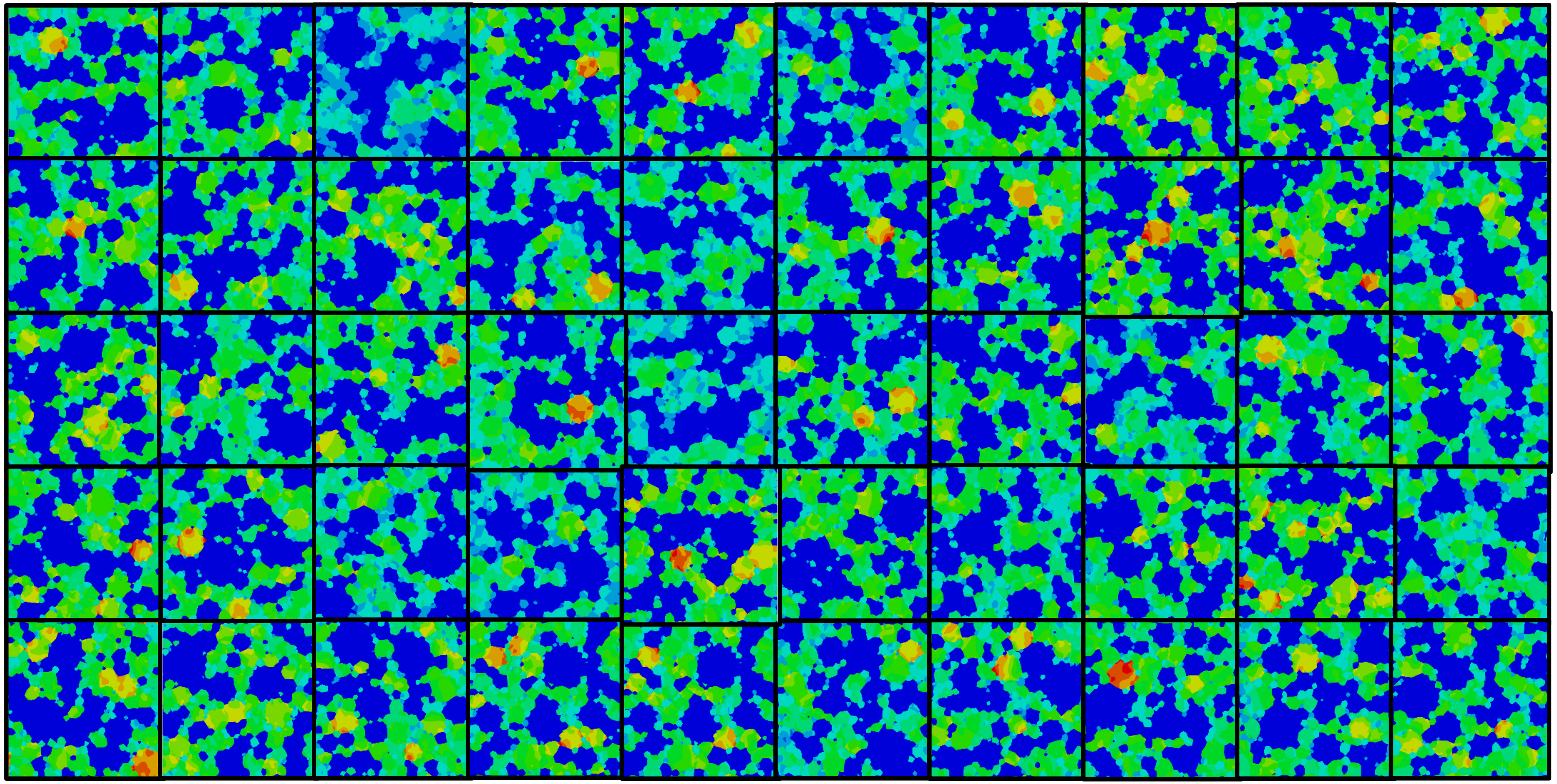

Parameter extraction

Grain size averaged accumulated plastic strain P_{mps}:

$$P_{mps} = \max\left(\frac{1}{\sum_{i=1}^{N_E^{Gr}} V_i^{Gr}} \sum_{i=1}^{N_E^{Gr}} p_i V_i^{Gr}\right).$$

W. D. Musinski, D. L. McDowell, Microstructure-sensitive probabilistic modeling of hcf crack initiation and early crack growth in ni-base superalloy in100 notched components, International Journal of Fatigue 37 (2012) 41–53. doi:10.1016/j.ijfatigue.2011.09.014.

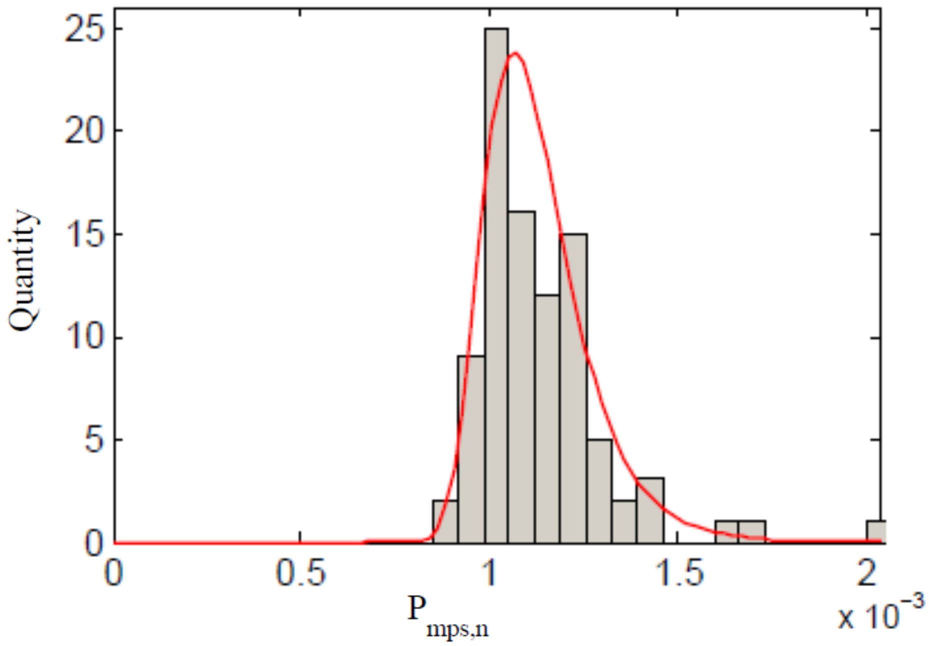

Histogram of extracted grain size average accumulated plastic strain extreme values of 94 RVEs with same loading conditions; set definition: σ_a = 402 MPa and R= -1

The parameter was extracted from each RVE which has been loaded with the same loading level and stress ratio.

Sensitivity of the lifetime prediction equations

$$N_{inc,i} = \frac{\alpha_p}{d_{gr}(\Delta P_{mps,mv,i})^2}$$

$$N_{HCF,i} = N_{inc,i}\left(1 + \frac{\sum_i^N (A_i B_i)^u \sigma_i}{(A_i B_i)^u \sum_i^N \sigma_i}\right)$$

Calibration of the constants

- Changing α_p: parallel shift of $N_{HCF,i}$ values to higher cycle numbers.
- Changing u: tilt of $N_{HCF,i}$values.

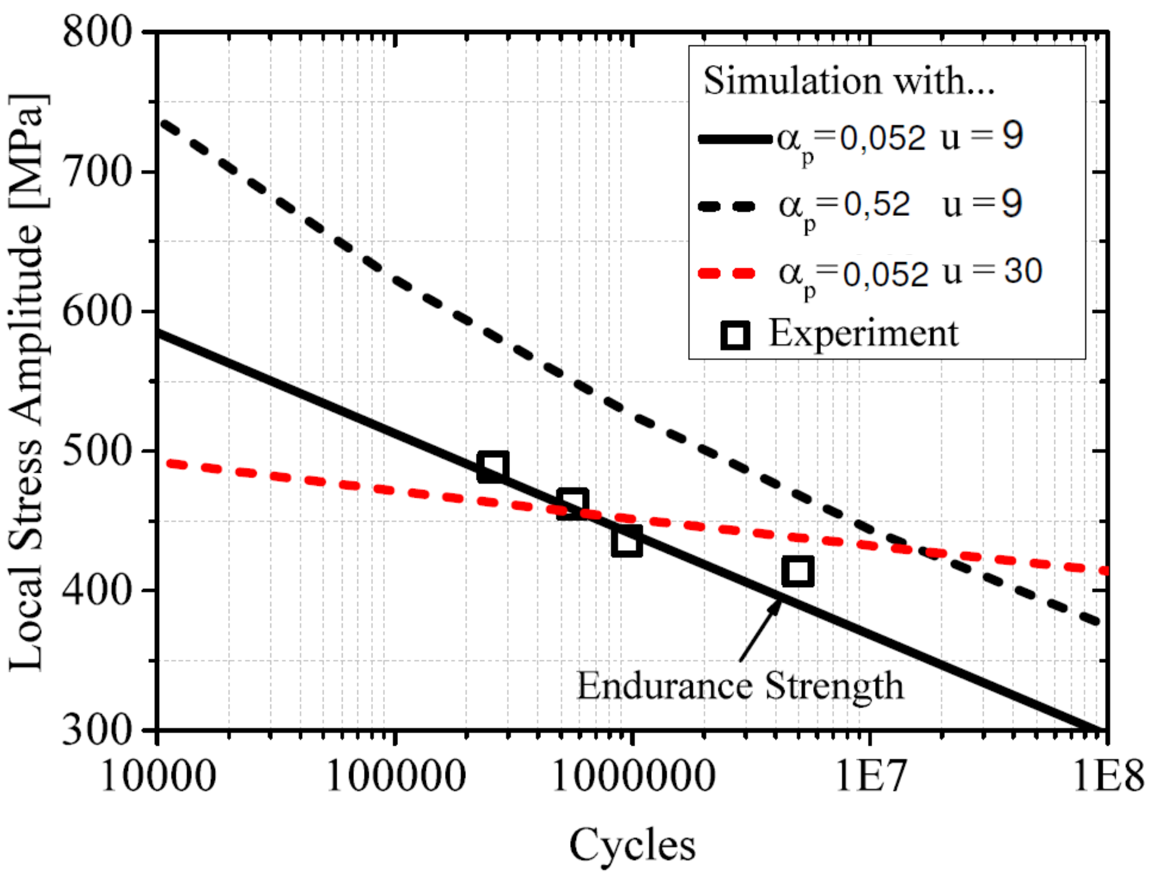

Local SN-plot of experimental and simulation results: Square symbols are the 50% fracture probability of the experiments, determined with notched specimens, R=-1, 35 Hz; solid line is best fit of parameters; dotted lines are derivative parameter sets

Validation of the prediction approach: R-Values

Material
- 38MnSiV5
- “No” initiation at inclusions

Experimental details:
- Tests for calibration with
- R=-1;
- Specimen notched
  K_t=1.45;
- 35 Hz

Tests for verification
- R=0.1;
- Specimen smooth
  K_t=1.02;
- 35 Hz

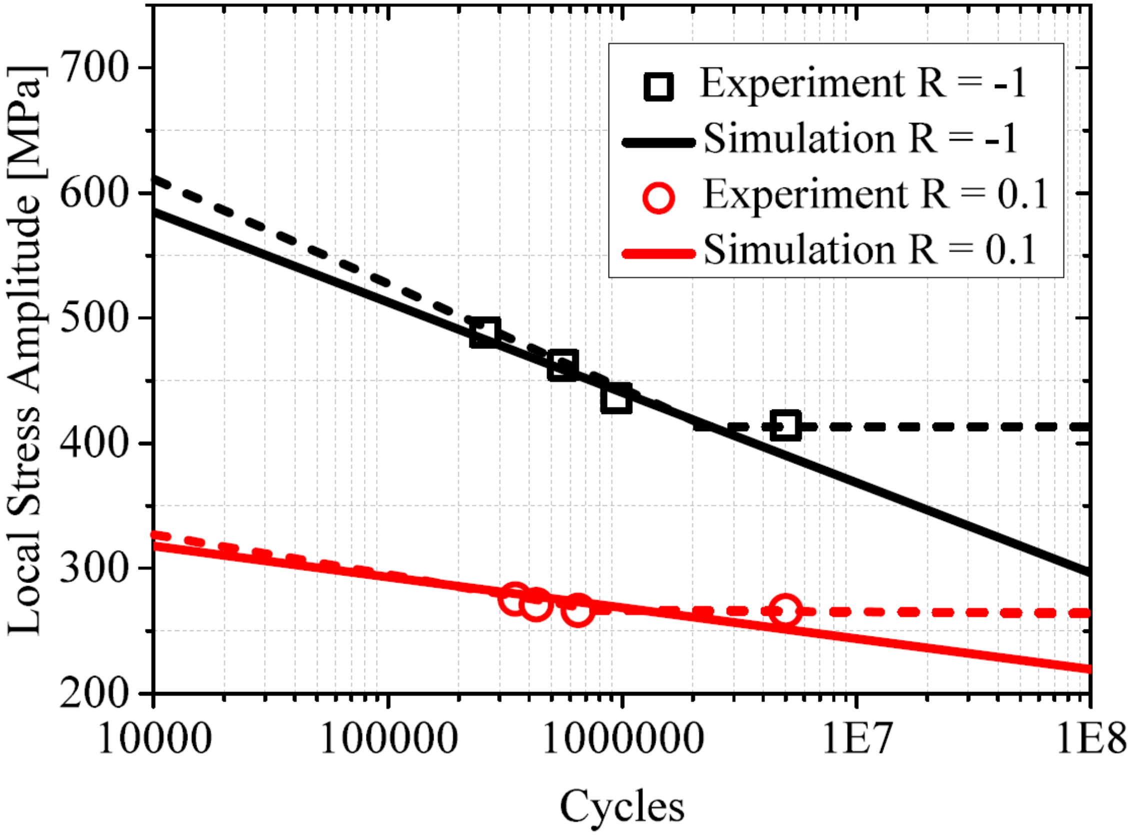

Local SN-plot of experimental and simulation values for different R-ratios; black squares are the experimental results of the fitting procedure; black dotted line is the 50% fracture probability SN- curve of the experiments; black curve is the simulated SN-curve; round red symbols and dotted line are the 50% fracture probability of experiments with R=0.1, hourglass specimen, 35Hz; red line is the simulated SN-curve

Residual stresses around inclusions

Material	Coefficient of linear expansion, α / 10^{-6} °C	Young's modulus, E / GPa	Poisson's ratio, v
Al_2O_3	8.0	390	0.25
$MgO\text{-}Al_2O_3$	8.4	271	0.26
MnS	14.8	103	0.30
TiN	9.4	320	0.19
Steel matrix	23.0	206	0.30

Effect of cooling after hot rolling

- Both matrix and inclusions shrink due to temperature decrease
- Incompatibility of thermal expansion coefficients leads to residual stresses
- In most cases, tensile stress in the steel matrix, compressive stress in the particle

Application of concept – attempt #2

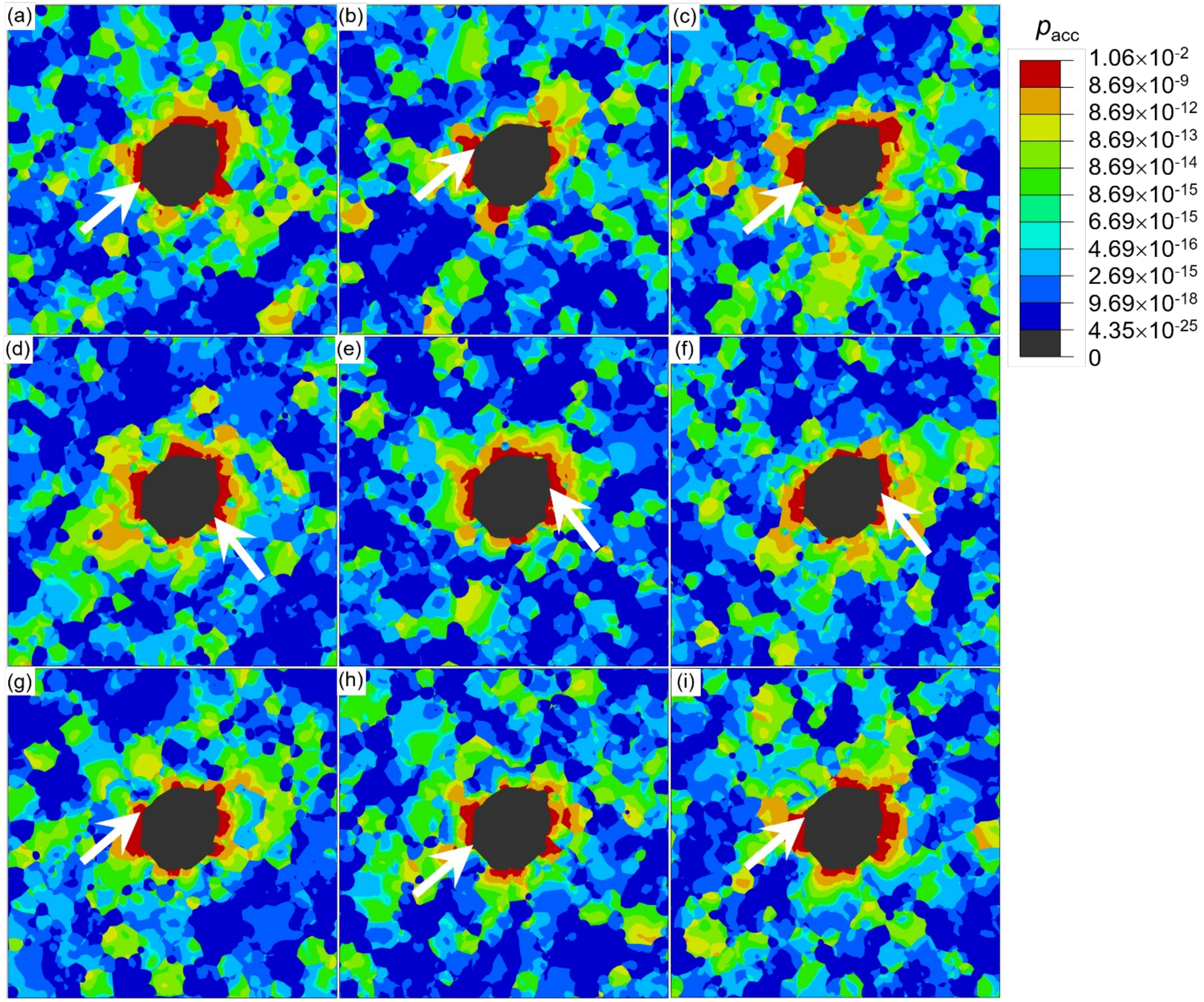

Predicted fatigue lifetime

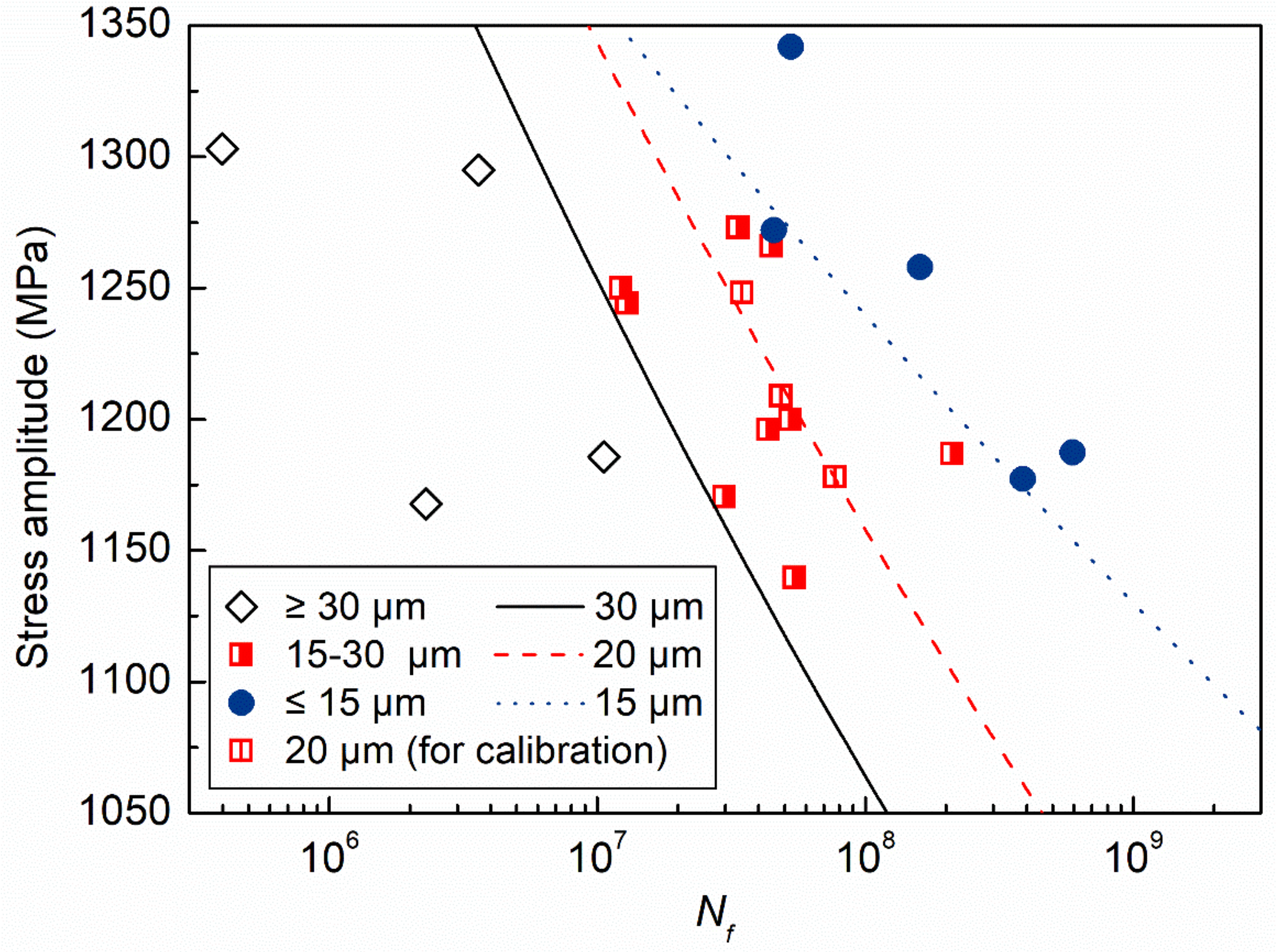

Example 2: Edge crack sensitivity

How does the manufacturing of edges affect the edge crack resistance?

Edge crack sensitivity

- Cracks occuring during edge forming operations
- No correlation to fracture elongation or uniform elongation
- Known influencing factors:
  → Manufacturing processes
  → Microstructure
- Common experimental characterization approach: Hole expansion test

$$HER = \frac{D_0 - D_H}{D_0} * 100$$

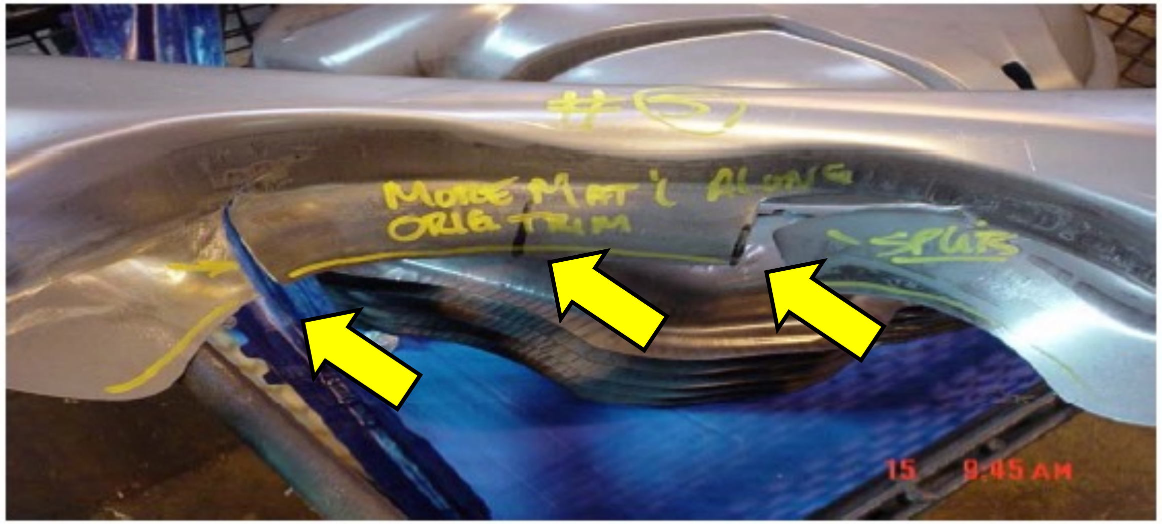

Shi and Chen, SAE Int., 2007

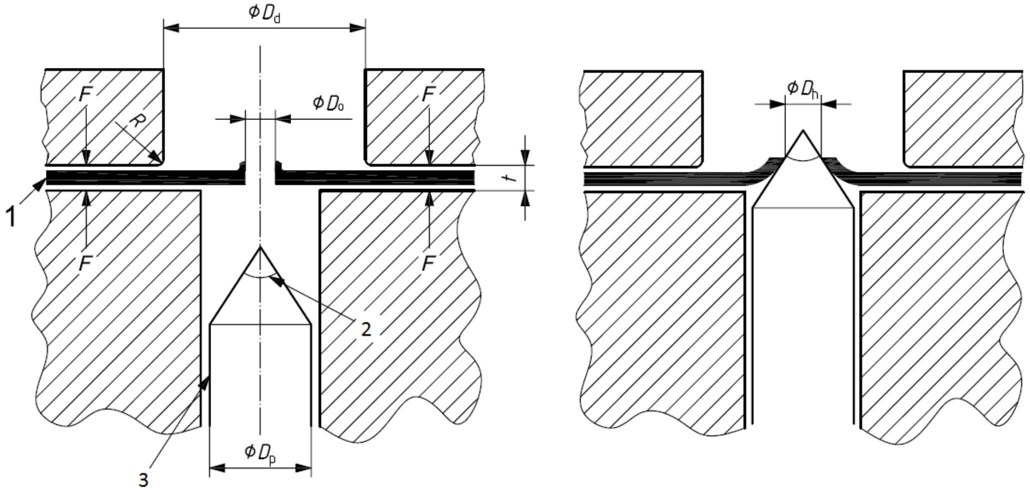

MBW model

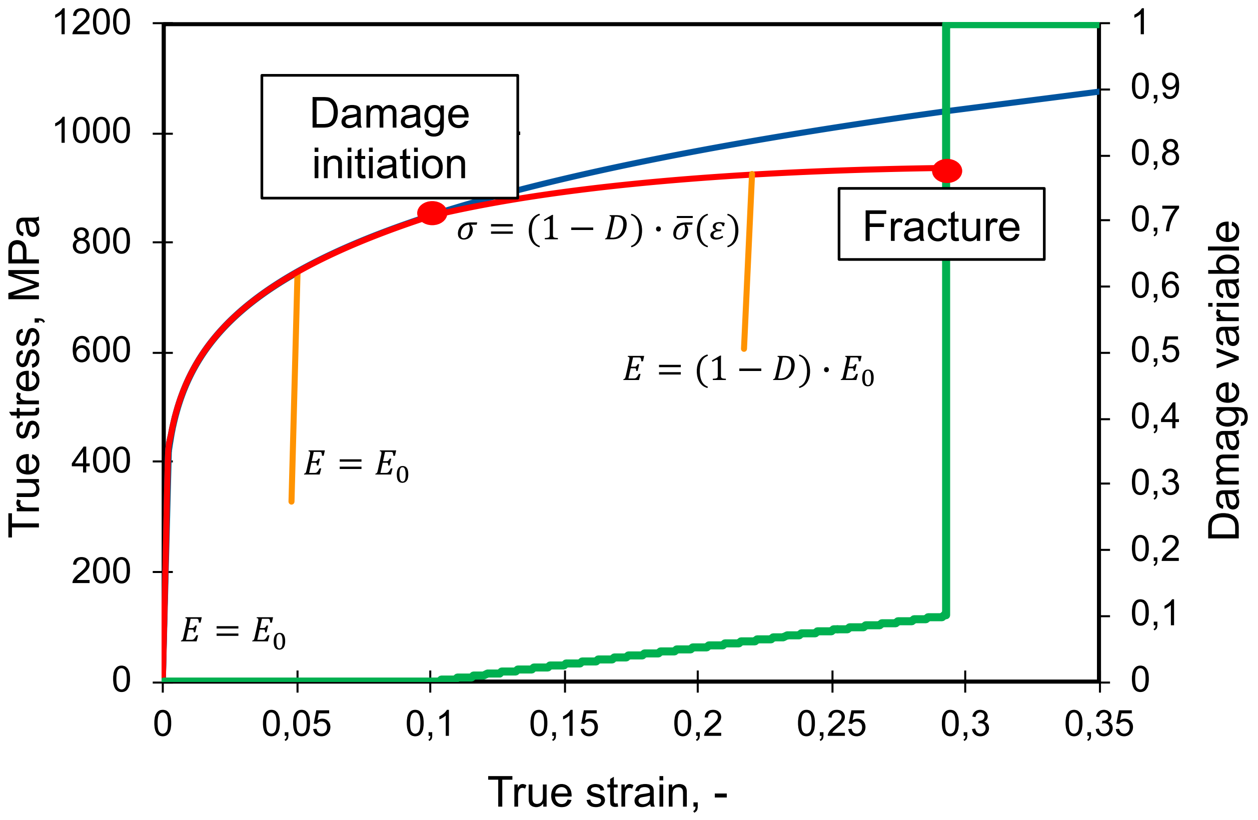

1200
1000
800
600
400
200
0
True stress, MPa
0
0,05
0,1
0,15
0,2
0,25
0,3
0,35
True strain, -
1
0,9
0,8
0,7
0,6
0,5
0,4
0,3
0,2
0,1
0
Damage variable
Damage initiation
Fracture
$\sigma = (1 - D) \cdot \bar{\sigma}(\varepsilon)$
$E = (1 - D) \cdot E_0$
$E = E_0$
$E = E_0$

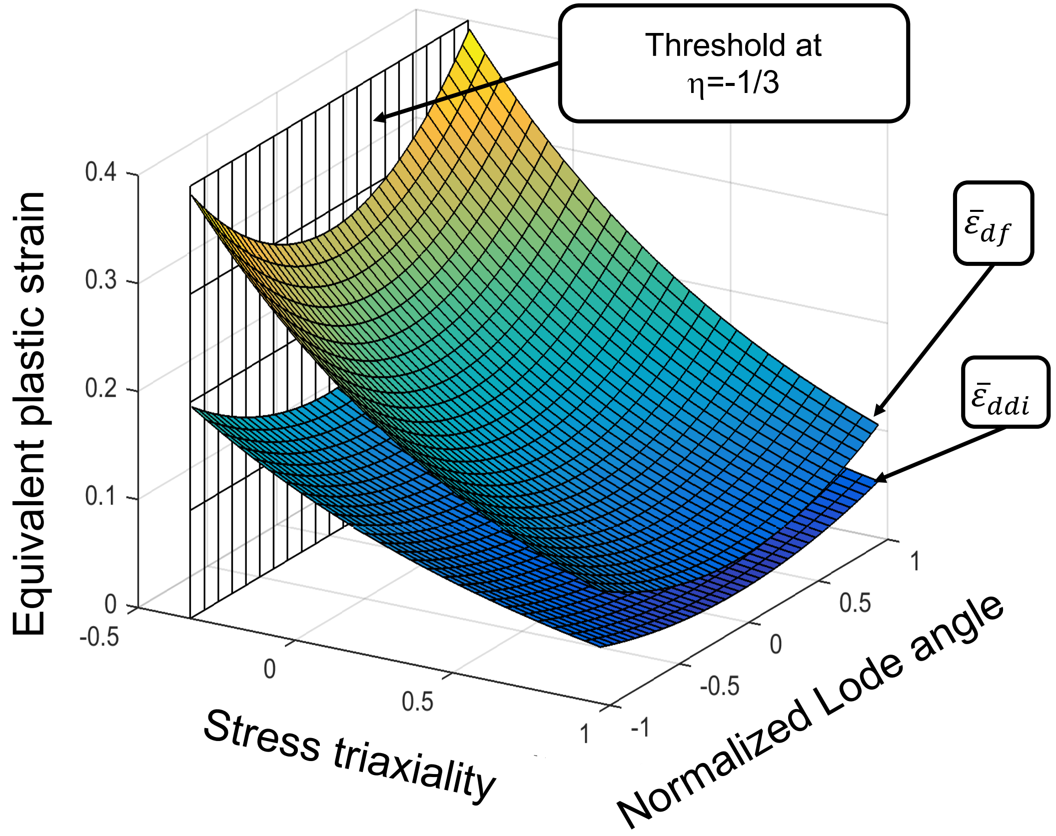

Threshold at η=-1/3
$\bar{\varepsilon}_{df}$
$\bar{\varepsilon}_{ddi}$
Equivalent plastic strain
0.4
0.3
0.2
0.1
0
-0.5
0
0.5
1
Stress triaxiality
-1
-0.5
0
0.5
1
Normalized Lode angle

Simulation of hole expansion test

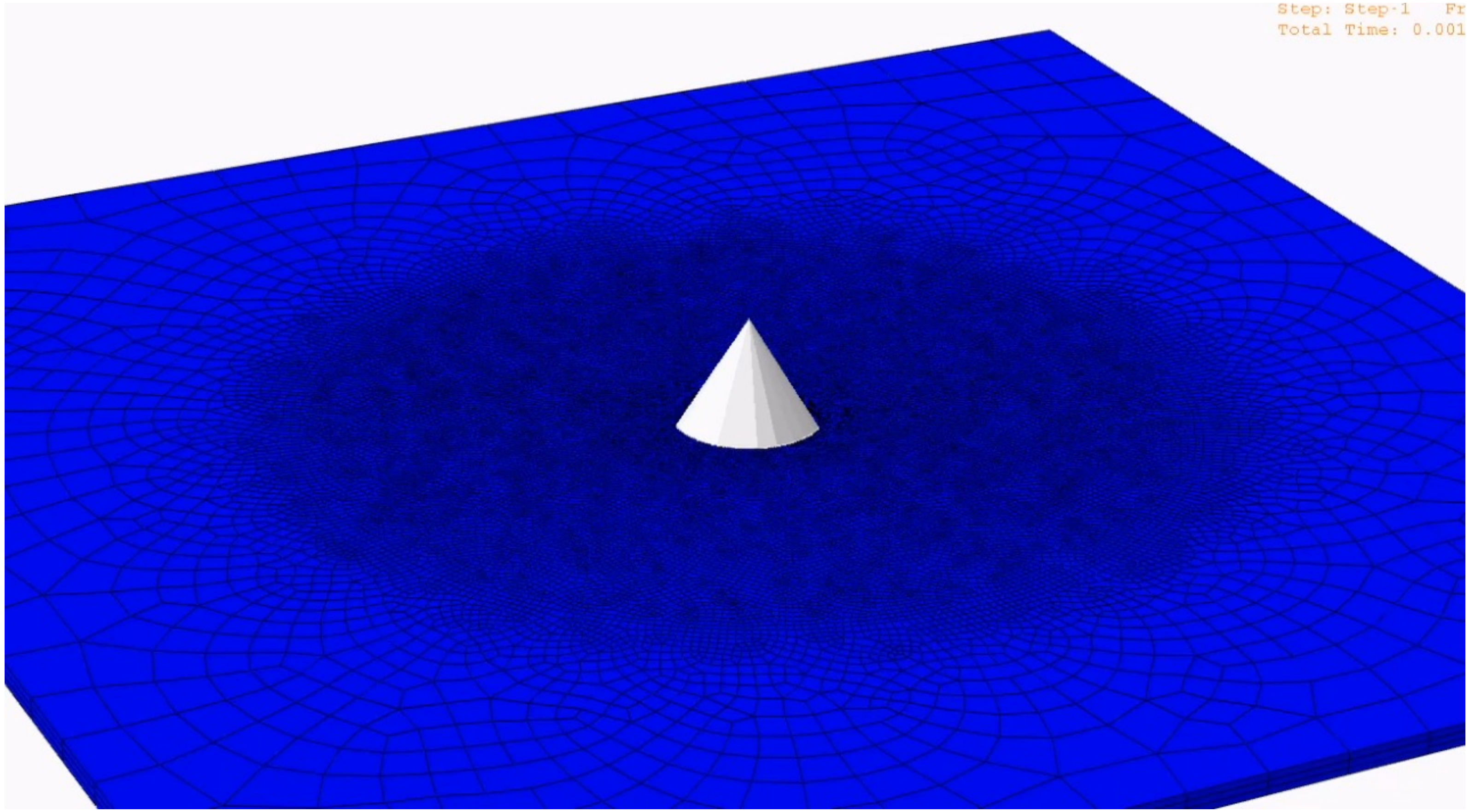

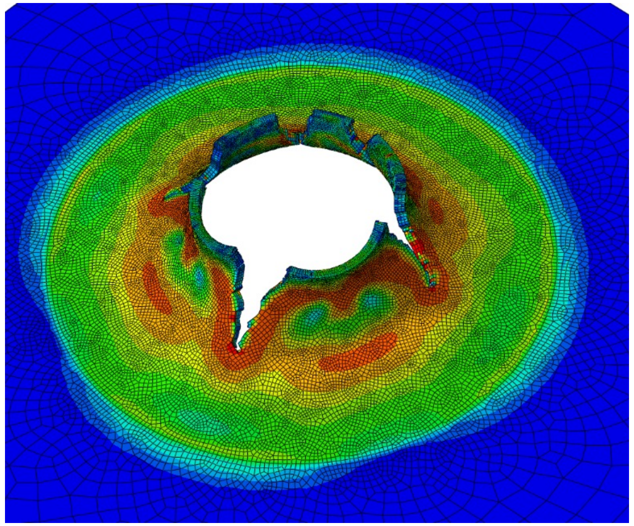

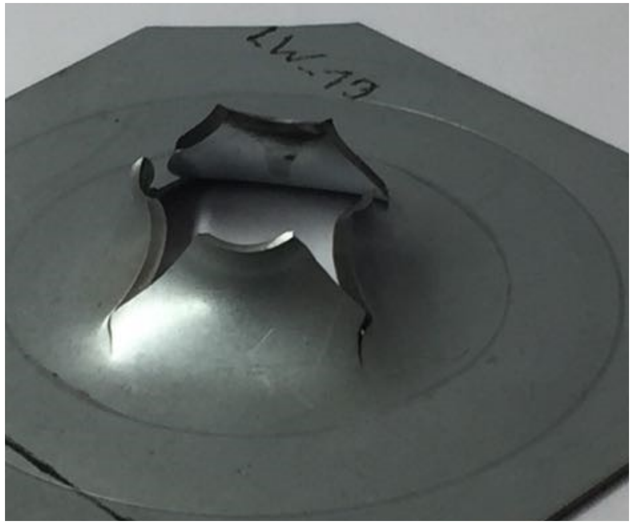

Evaluation of HER

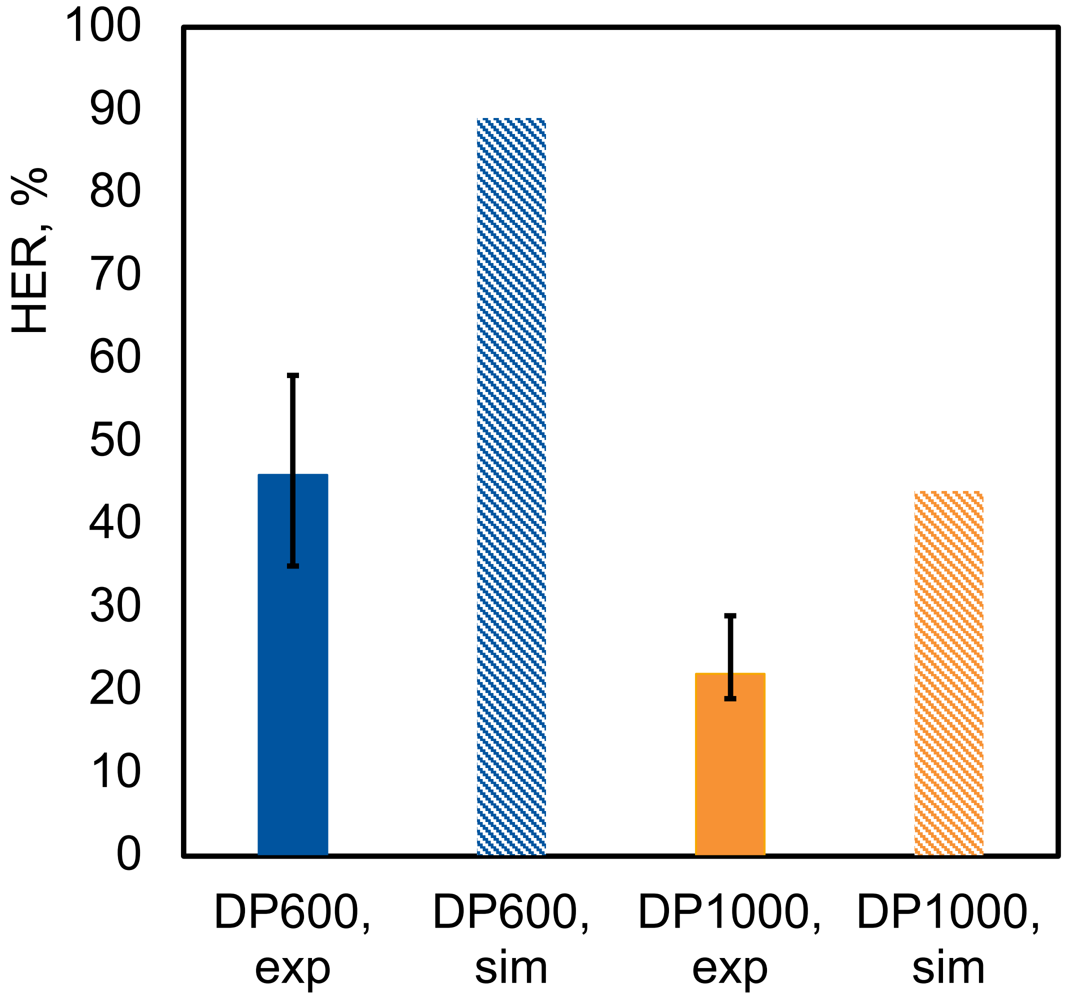

Scratches and roughness decrease edge formability…

- …due to strain localization
- ... due to transformation to less favourable stress states

Macroscopic ductile damage mechanics models cannot capture these effects

- Assumption of smooth surfaces,
- Roughness profiles significantly below FE edge length

Residual damage from manufacturing

- Depending on microstructure
- Relevant for any kind of shear cutting

Experimental results

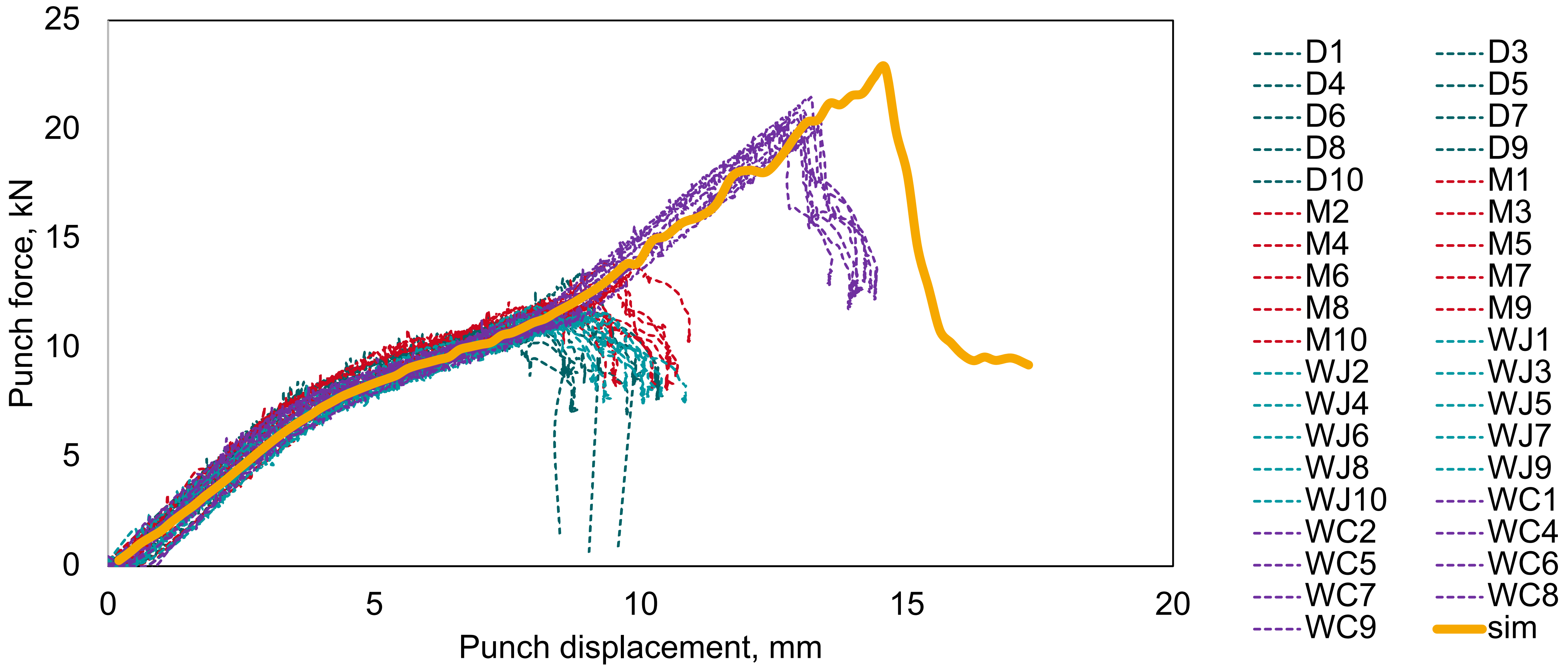

Roughness profiles resulting from different manufacturing processes

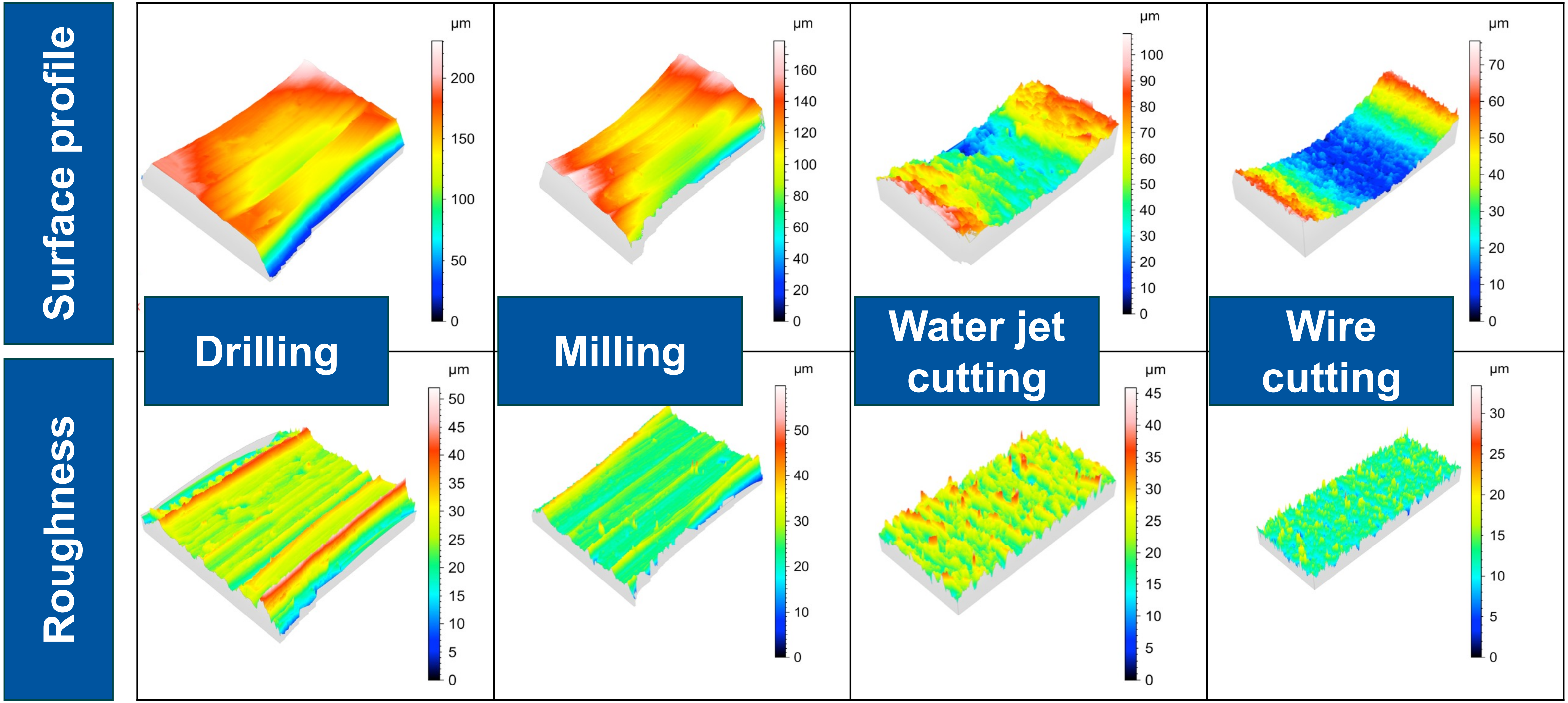

Roughness and waviness (before test is started)

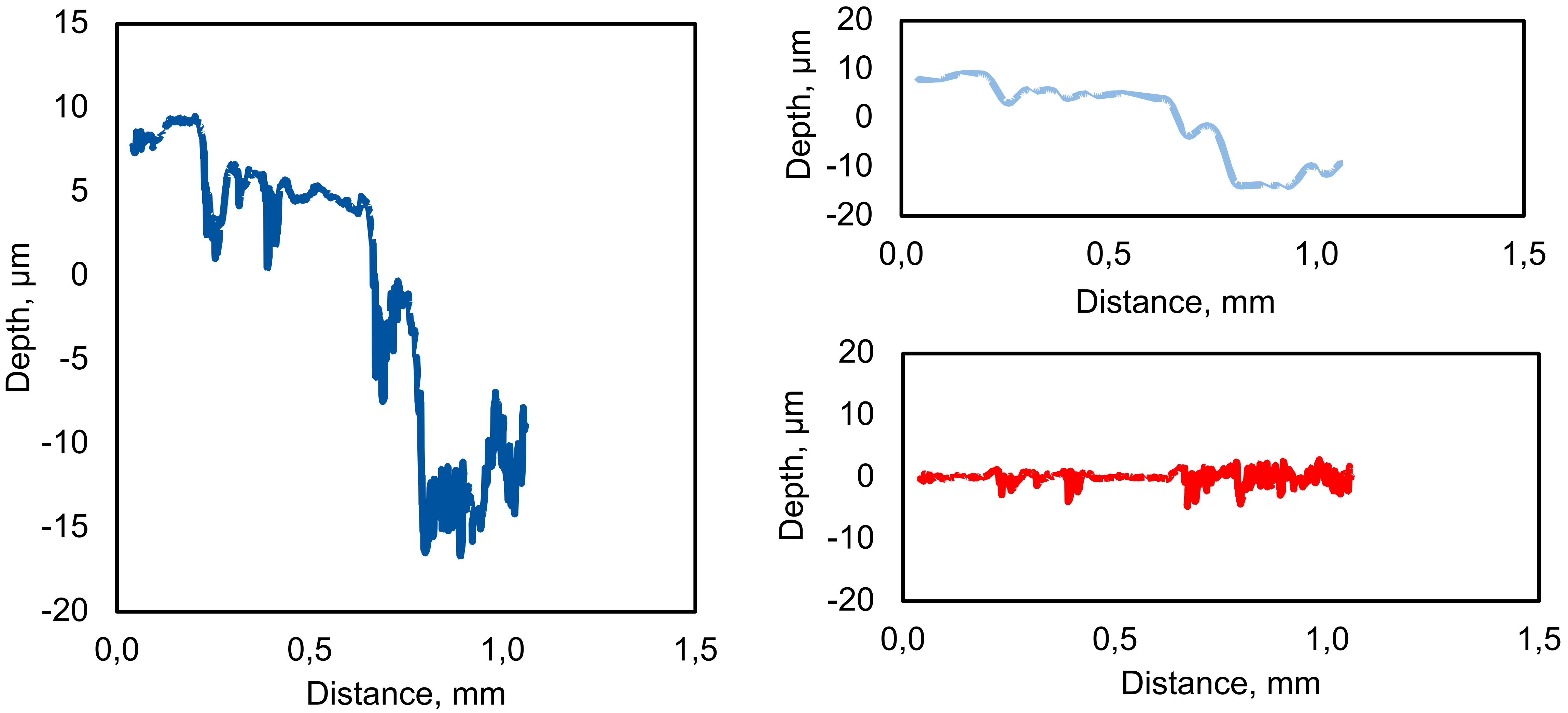

Construction of submodels

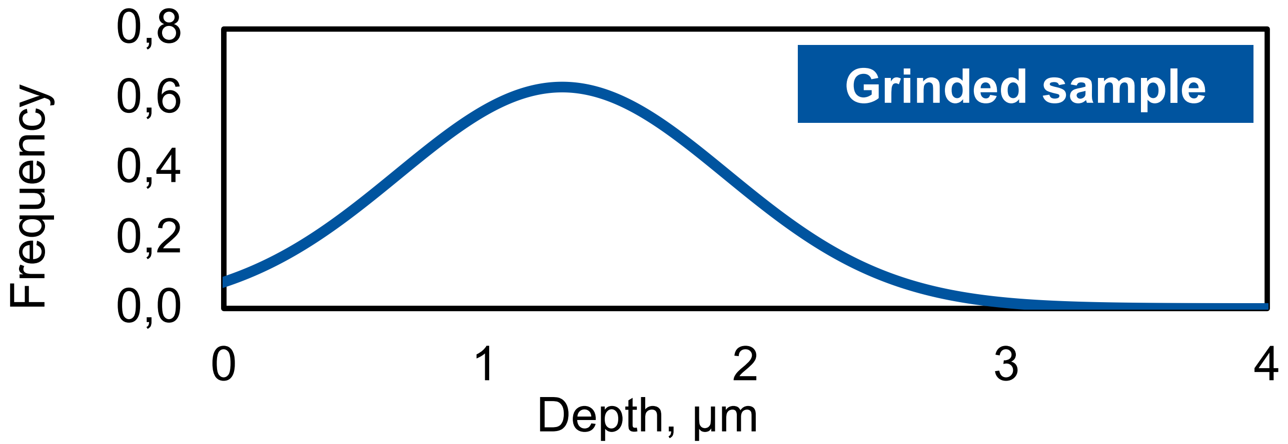

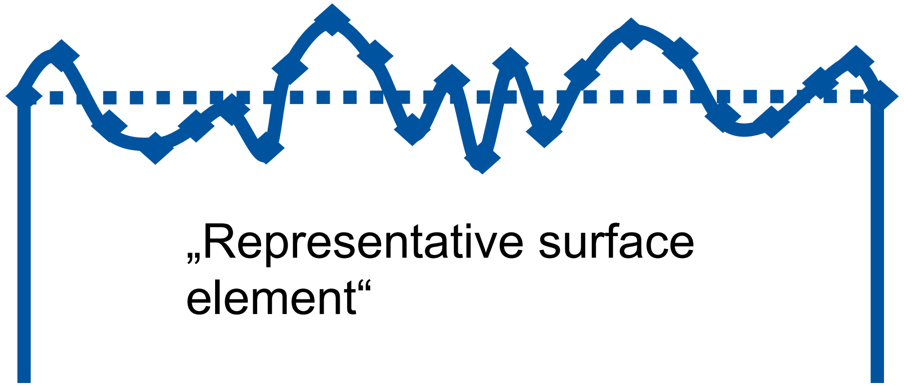

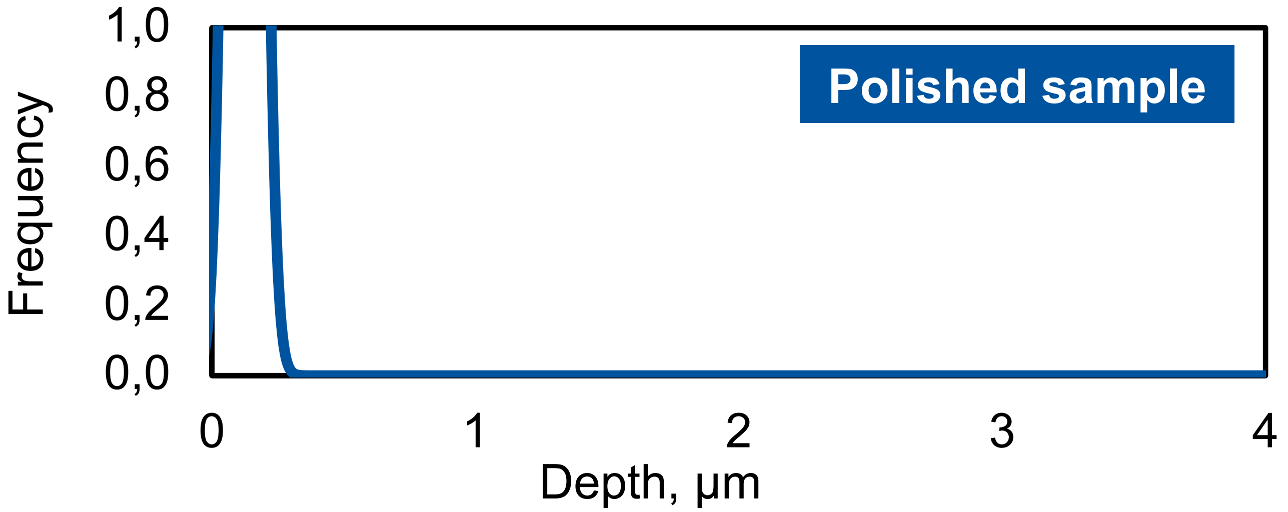

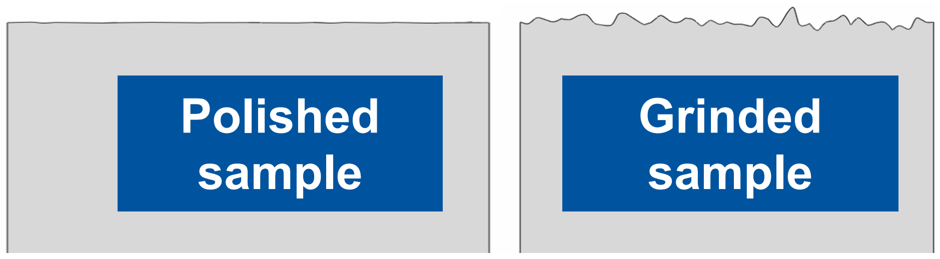

Simulation results (micro scale)

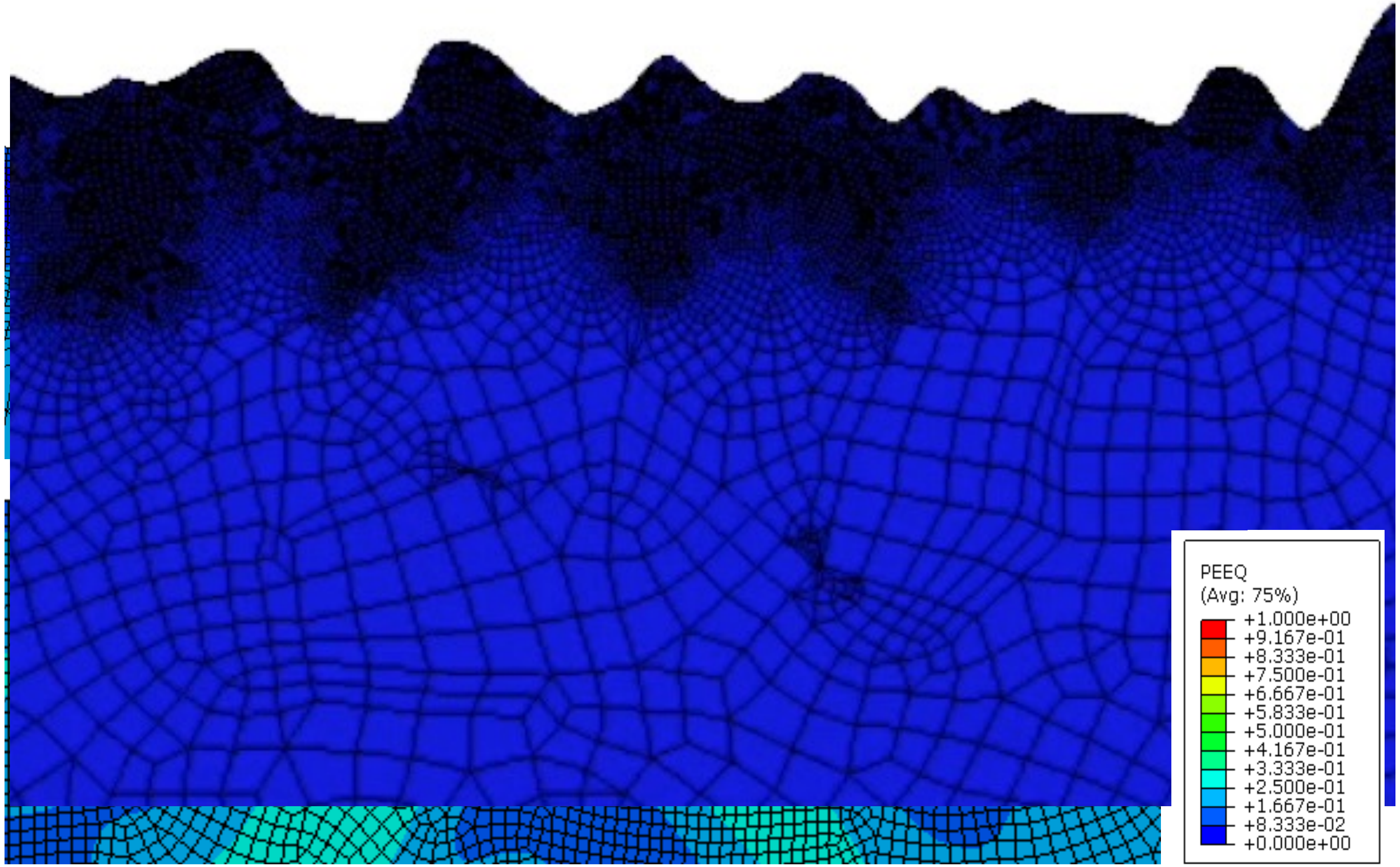

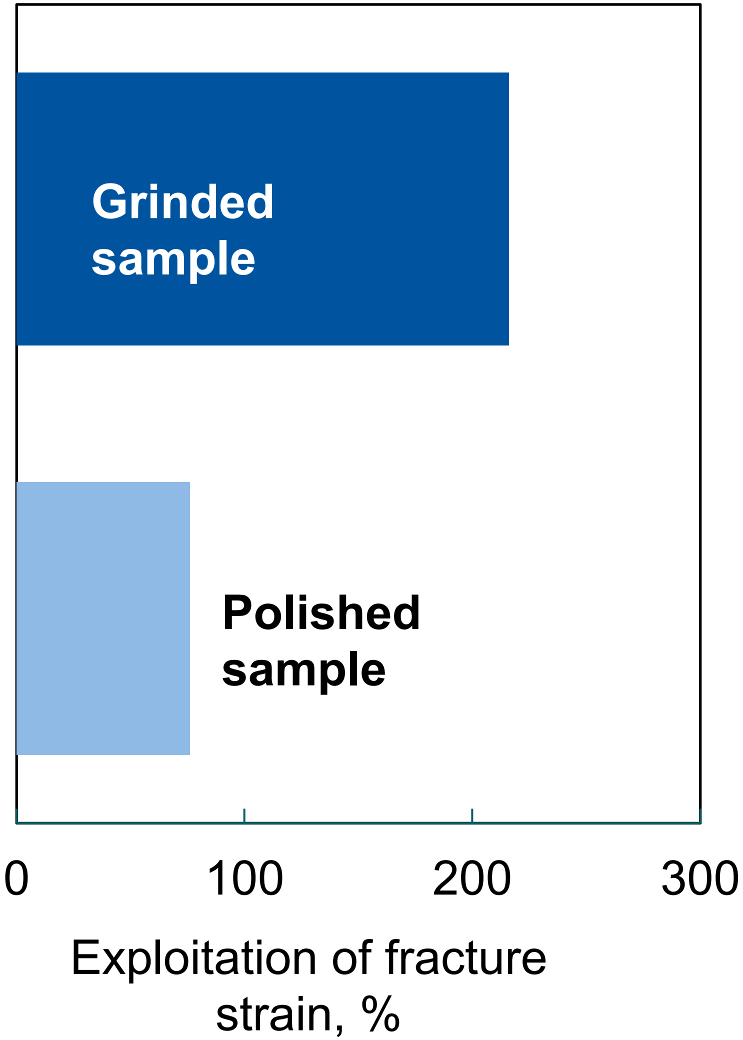

Comparison experiment-simulation

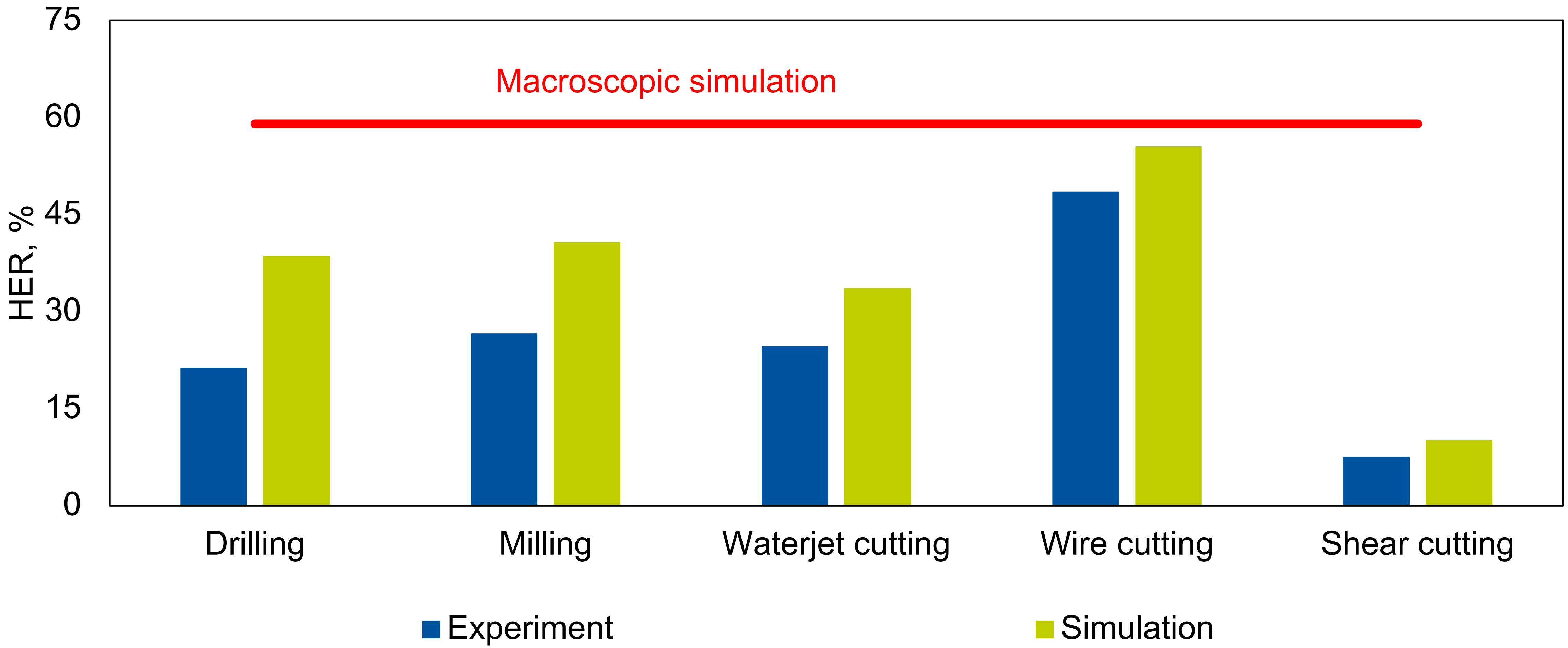

Example 3: Texture design for cold formability

How does the process-induced crystallographic texture affect the sheet material´s cold formability?

Material property characterization
Texture – AISI 439

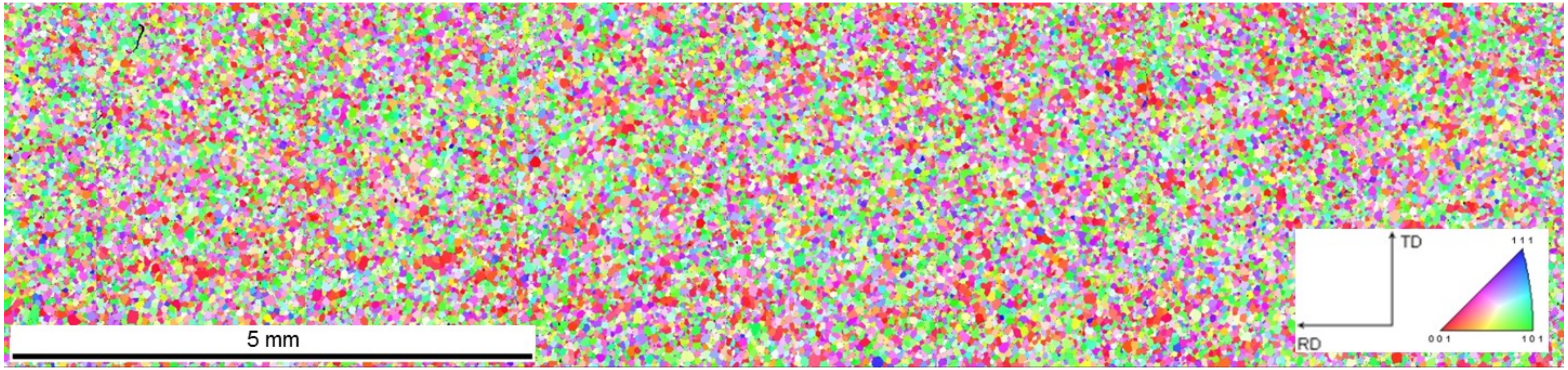

- Material: AISI 439 ferritic stainless sheet steel
- Sample size: 3.5 mm*15 mm
- 8 measurements in mid thickness stitched to one figure
- Total grain number: 41,119
- Number of α grains: 41,105
- Number of grains inside the scanning area: 40,434
- Number of α grains inside the scanning area: 40,420

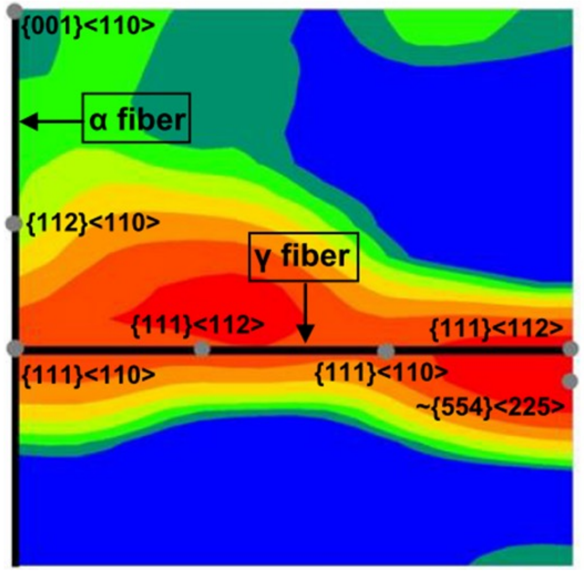

Material property characterization
Tensile properties and formability – AISI 439

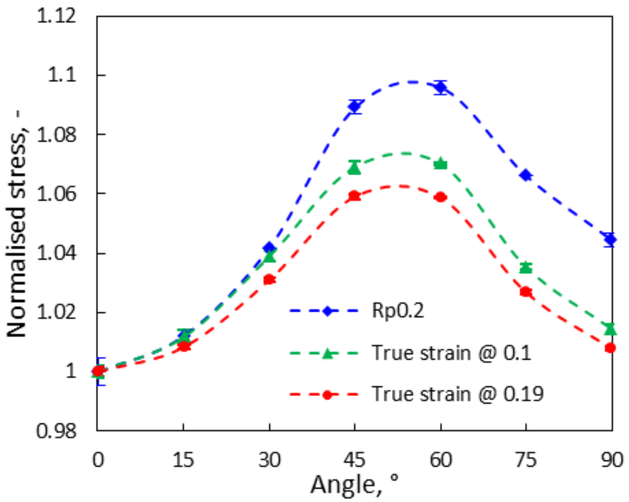

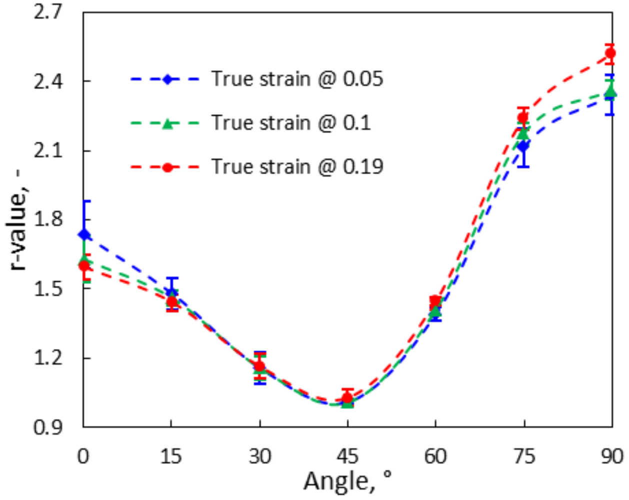

- **Anisotropy evolution**
  - Obvious anisotropy for the initial yield stress and the initial r-values
  - Significant evolution of flow stress anisotropy due to anisotropic strain hardening
  - Only minor evolution of r-value anisotropy with

- Nakajima tests according to ISO 12004-2
- Sample size: 190 mm * web width mm
- 3-layer lubrication system
- Evaluations methods:
  Visual method & Position dependent method

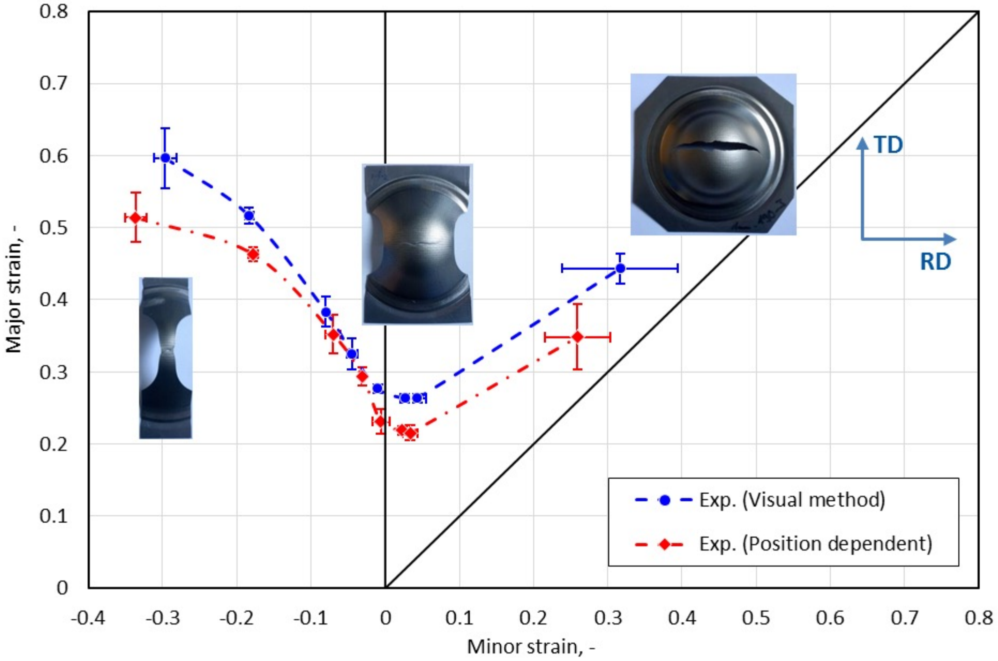

Alternative approach: Virtual experiments on RVE

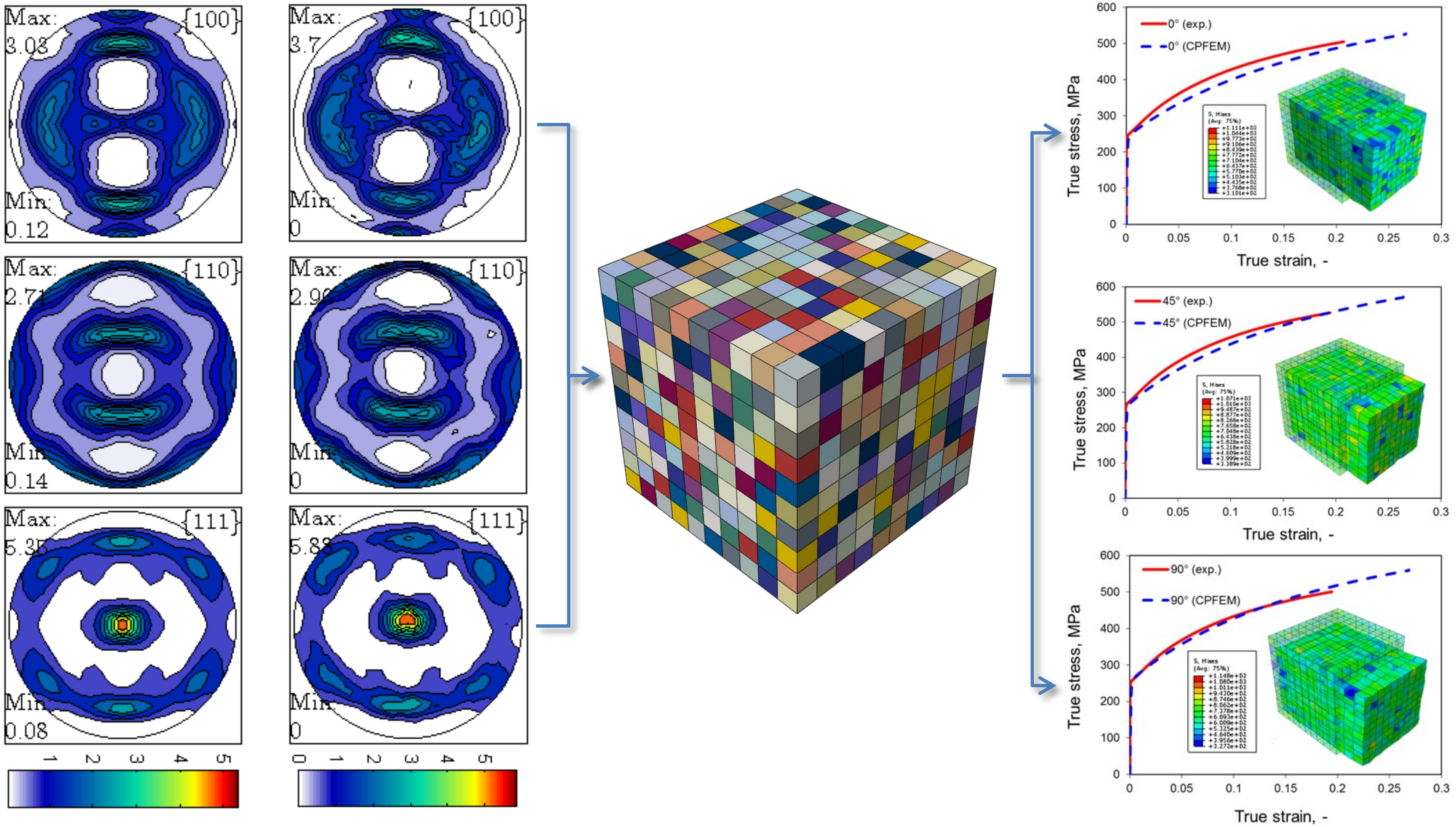

Original texture | **Reduced texture** | **RVE with assigned texture** | **Virtual laboratory**

Challenges, solution approach

Challenges

- Hill48 model is even not capable to reproduce anisotropy of r-value and yield stress at the same time
- py
  ing

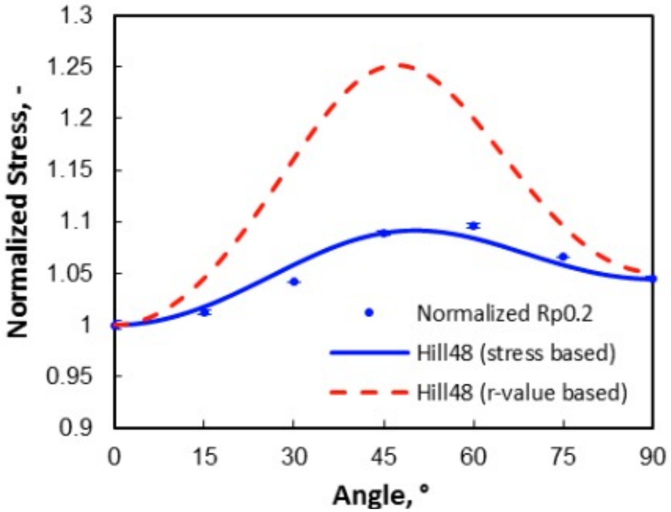

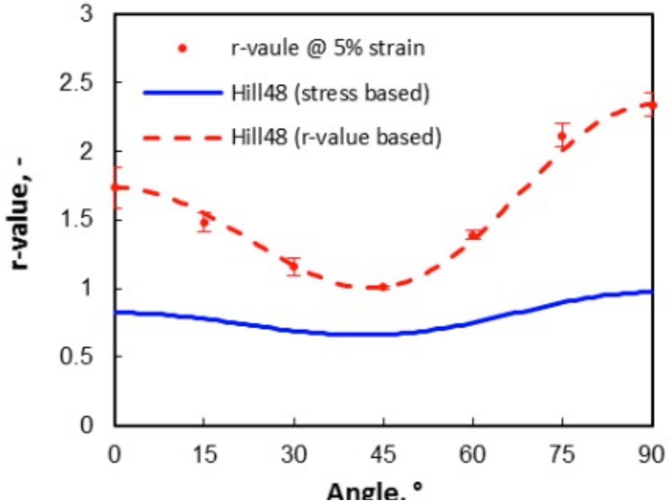

So

- es
- Define all material parameters as functions of equivalent plastic strain.
- Details in Lian et al., IJSS 2017

Evolving non-associated Hill48 (enHill48) model
Lian et al., IJSS, 2017

Yield function:

$$f = \bar{\sigma}(\boldsymbol{\sigma}) - \sigma_{\mathrm{Y}}(\bar{\varepsilon}^{\mathrm{p}}) \leq 0$$

$$F_\sigma(\bar{\varepsilon}^p) = \frac{\sigma_0^2(\bar{\varepsilon}^p)}{\sigma_{90}^2(\bar{\varepsilon}^p)} - 1 + \frac{\sigma_0^2(\bar{\varepsilon}^p)}{\sigma_b^2(\bar{\varepsilon}^p)},$$

$$G_\sigma(\bar{\varepsilon}^p) = 1 - \frac{\sigma_0^2(\bar{\varepsilon}^p)}{\sigma_{90}^2(\bar{\varepsilon}^p)} + \frac{\sigma_0^2(\bar{\varepsilon}^p)}{\sigma_b^2(\bar{\varepsilon}^p)},$$

$$H_\sigma(\bar{\varepsilon}^p) = 1 + \frac{\sigma_0^2(\bar{\varepsilon}^p)}{\sigma_{90}^2(\bar{\varepsilon}^p)} - \frac{\sigma_0^2(\bar{\varepsilon}^p)}{\sigma_b^2(\bar{\varepsilon}^p)},$$

$$L_\sigma(\bar{\varepsilon}^p) = 3,$$

$$M_\sigma(\bar{\varepsilon}^p) = 3,$$

$$N_\sigma(\bar{\varepsilon}^p) = \frac{4\sigma_0^2(\bar{\varepsilon}^p)}{\sigma_{45}^2(\bar{\varepsilon}^p)} - \frac{\sigma_0^2(\bar{\varepsilon}^p)}{\sigma_b^2(\bar{\varepsilon}^p)}$$

Flow potential:

$$g = \bar{\sigma}(\boldsymbol{\sigma}) - \sigma_{\mathrm{Y}}(\bar{\varepsilon}^{\mathrm{p}}) \leq 0$$

$$F_r(\bar{\varepsilon}^p) = \frac{2r_0(\bar{\varepsilon}^p)}{r_{90}(\bar{\varepsilon}^p)\big(1 + r_0(\bar{\varepsilon}^p)\big)},$$

$$G_r(\bar{\varepsilon}^p) = \frac{2}{1 + r_0(\bar{\varepsilon}^p)},$$

$$H_r(\bar{\varepsilon}^p) = \frac{2r_0(\bar{\varepsilon}^p)}{1 + r_0(\bar{\varepsilon}^p)},$$

$$L_r(\bar{\varepsilon}^p) = 3,$$

$$M_r(\bar{\varepsilon}^p) = 3,$$

$$N_r(\bar{\varepsilon}^p) = \frac{\big(r_{90}(\bar{\varepsilon}^p) + r_0(\bar{\varepsilon}^p)\big)(1 + 2r_{45}(\bar{\varepsilon}^p))}{r_{90}(\bar{\varepsilon}^p)\big(1 + r_0(\bar{\varepsilon}^p)\big)}$$

Modified maximum force criterion (MMFC) (Hora, et al., IJMF, 2013)

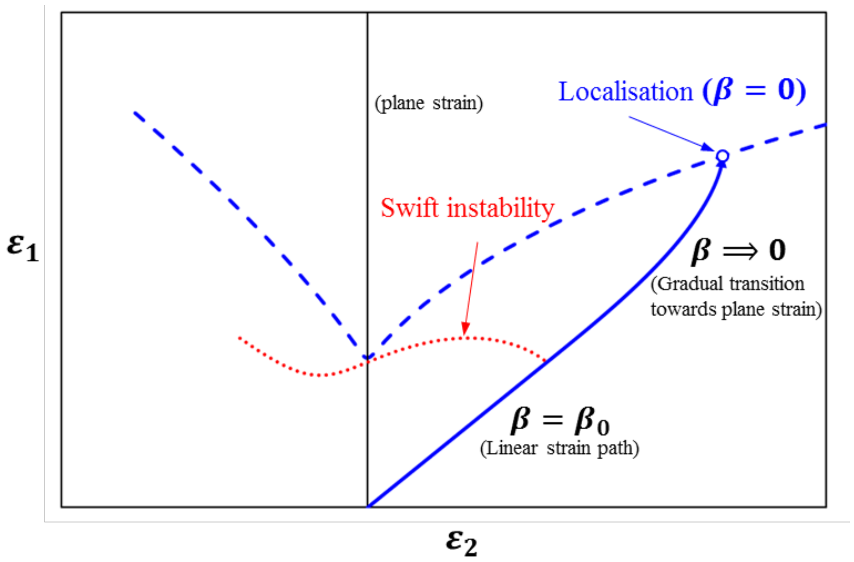

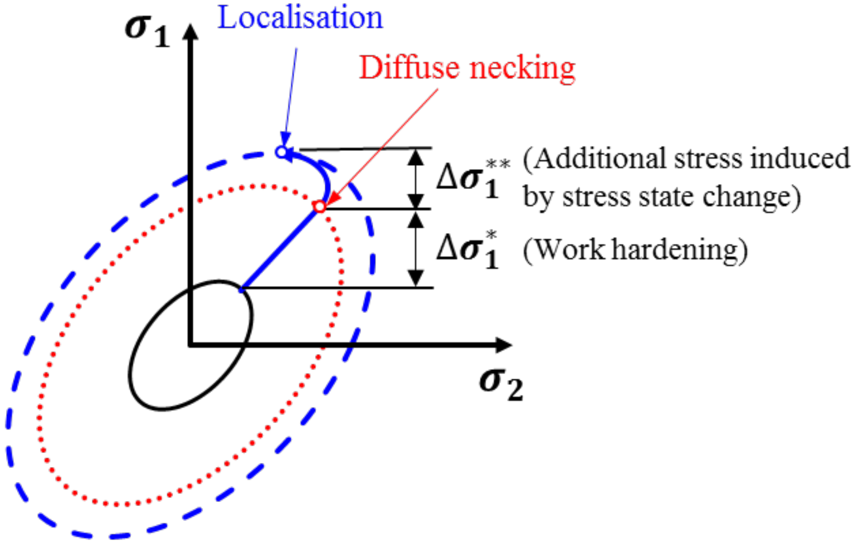

Derivation from the Maximum Force Criterion

$$(1)\ dF = d(\sigma_{11} \cdot A) = d\sigma_{11} \cdot A + \sigma_{11} \cdot dA = 0$$

$$(2)\ d\sigma_{11} = \sigma_{11} \cdot d\varepsilon_{11}$$

$$(3)\ d\sigma_{11} = \frac{\partial\sigma_{11}}{\partial\varepsilon_{11}} \cdot d\varepsilon_{11} + \frac{\partial\sigma_{11}}{\partial\beta} \cdot d\beta = \sigma_{11} \cdot d\varepsilon_{11}$$

$$(4)\ \frac{\partial\sigma_{11}}{\partial\varepsilon_{11}} + \frac{\partial\sigma_{11}}{\partial\beta} \cdot \frac{\partial\beta}{\partial\varepsilon_{11}} = \sigma_{11}$$

Variable definitions:

$$\alpha = \frac{\sigma_{22}}{\sigma_{11}};\ \beta = \frac{\dot{\varepsilon}_{22}}{\dot{\varepsilon}_{11}};\ f(\alpha) = \frac{\sigma_{11}}{\bar{\sigma}};\ g(\beta) = \frac{\bar{\varepsilon}^{\mathrm{p}}}{\varepsilon_{11}}$$

Strain state evolution:

$$\frac{\partial\beta}{\partial\varepsilon_{11}} = \frac{\sigma_{11} - f(\alpha) \cdot g(\beta) \cdot H'}{f'(\alpha) \cdot H / \frac{\partial\beta}{\partial\alpha}}$$

Parameter study: Effect of texture on cold formabilty

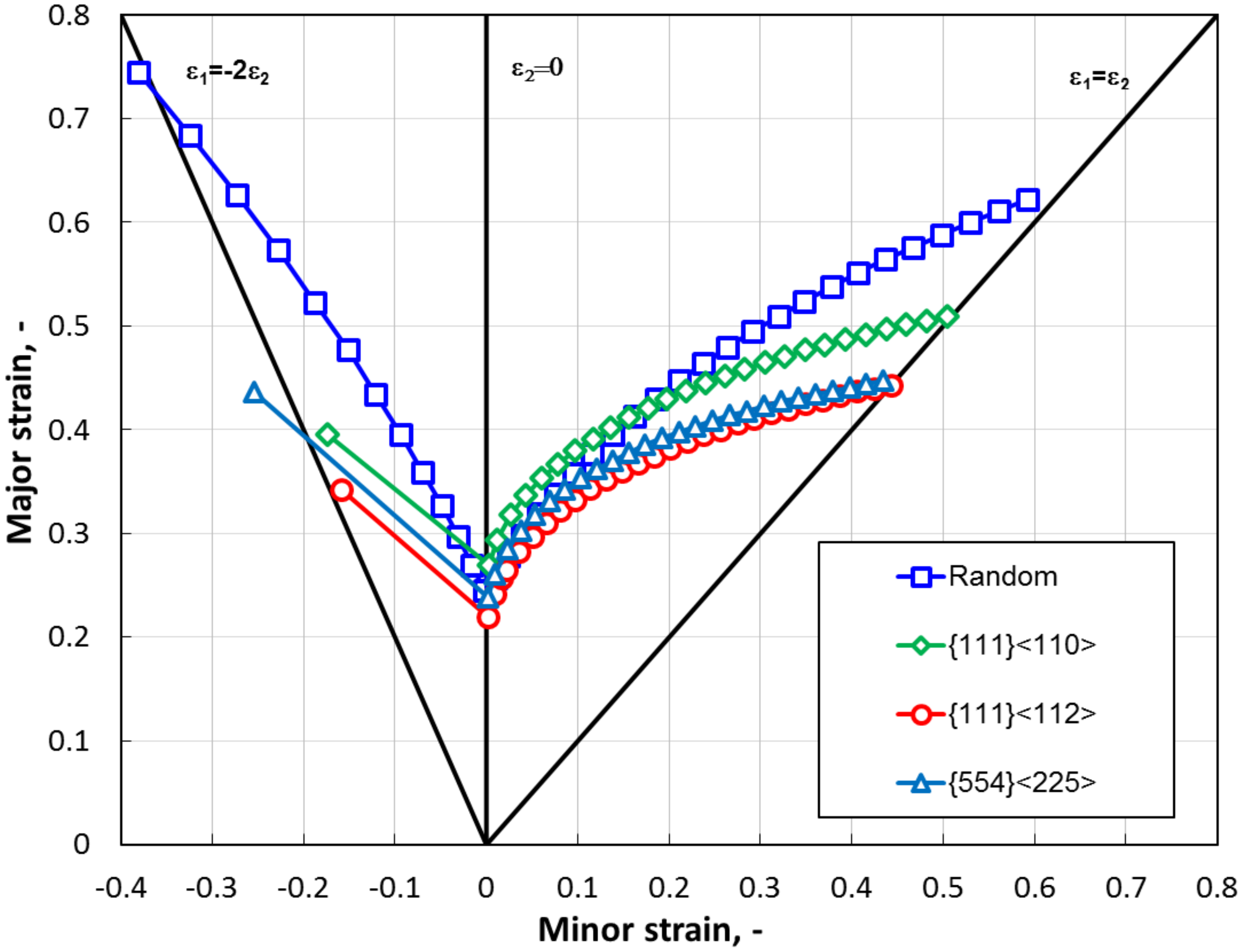

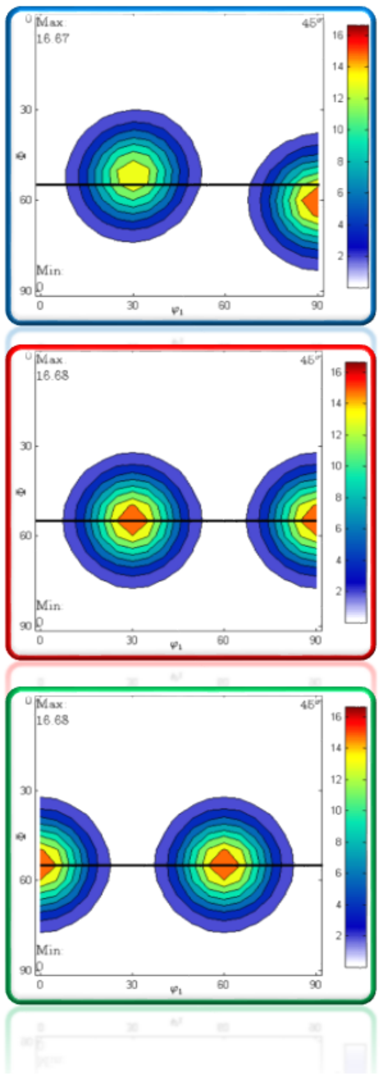

Example 4: Safety assessment for hydrogen infrastructure

How does the microstructure affect the resistance against hydrogen induced cracking?

Motivation - Strategy European Hydrogen Backbone 2022

Green Deal

REPowerEU

Fit for 55

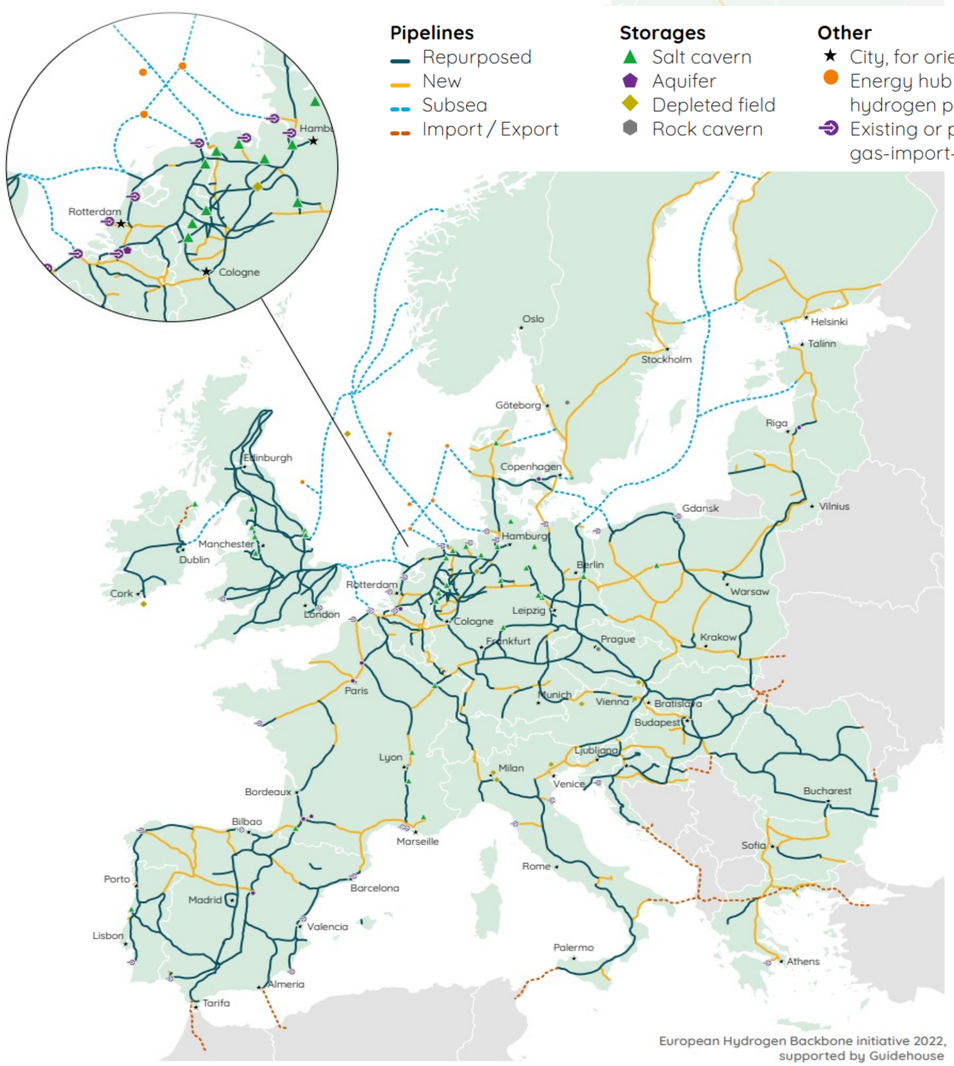

Until 2040:

- approx. 53.000 km pipeline network
- 60 % redesignated from pipelines for natural gas transport

Explosion craters Carlsbad 19.08.2000
(Quelle: NTSB/PAR-03/01)

Implementation of hydrogen diffusion according to Oriani

- Hydrogen diffusion can be described by Fick's laws
- Hydrogen atoms diffuse into areas of high elastic stress
- The hydrogen concentration is a function of hydrostatic stress
- Hydrogen atoms dissolved in the traps $\overset{!}{\Leftrightarrow}$ hydrogen atoms dissolved in the interstitial lattice sites.

Hydrogen traps

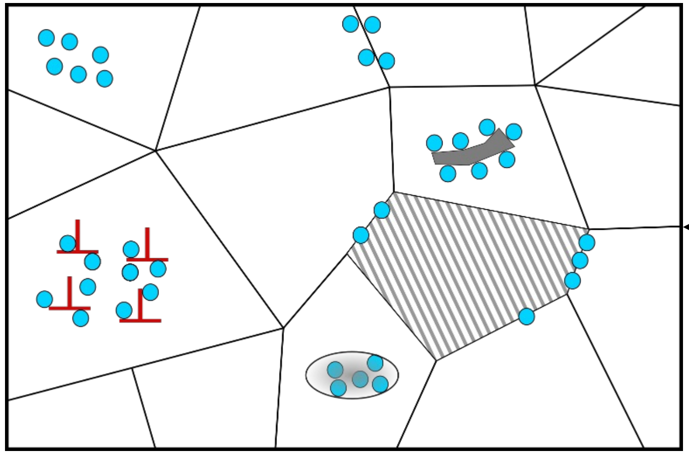

$$\underbrace{\frac{\partial \tilde{C}_L}{\partial t}\left[1+\frac{\partial \tilde{C}_T^d}{\partial \tilde{C}_L}+\frac{\partial \tilde{C}_T^{gb}}{\partial \tilde{C}_L}+\frac{\partial \tilde{C}_T^c}{\partial \tilde{C}_L}\right]}_{\text{Diffusion flux}} - \underbrace{\nabla_x \cdot \left[D_L \nabla_x \tilde{C}_L\right]}_{\text{Concentration difference over boundary}}$$

$$+\underbrace{\nabla_x \cdot \left[\frac{D_L \tilde{C}_L V_H}{RT} \nabla_x \sigma_H\right]}_{\text{Hydrogen concentration as a function of hydrostatic stress}} + \underbrace{\sum_i^d \frac{\partial \tilde{C}_T^i}{\partial \tilde{N}_T^i} \cdot \frac{\partial \tilde{N}_T^i}{\partial \varepsilon^p} \cdot \frac{d\varepsilon^p}{dt}}_{\text{Hydrogen concentration as a function of plastic strain}} = 0$$

Evolution of dislocation trap density

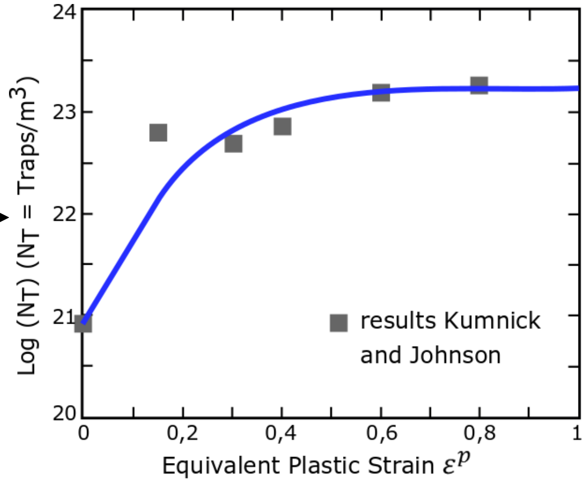

C_L = hydrogen in lattice sites;
V_H = partial molar volume of hydrogen;
N_T = available sites for hydrogen in traps;
K_T = equilibrium constant between lattice and trap sites

C_T = Hydrogen in trapes;
σ_H = hydrostatic stress;
N_L = available sites for hydrogen in lattice sites;

D_L = Diffusion coefficient;
R = universal gas constant;
ε_p = equivalent plastic strain;

Option 1:
Fracture locus under hydrogen loading $\bar{\varepsilon}_{df}(\eta_{avg}, \bar{\theta}_{avg}, C_{H^+})$

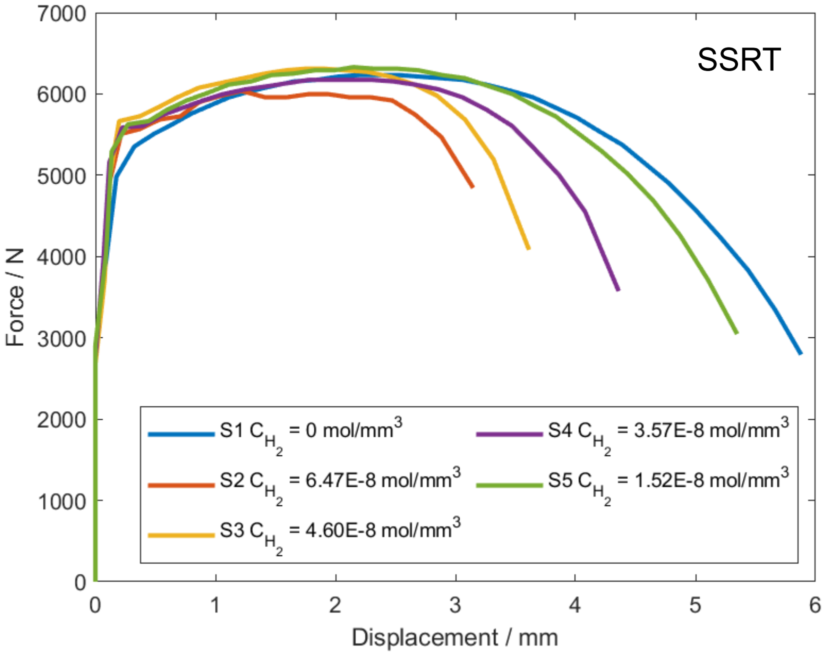

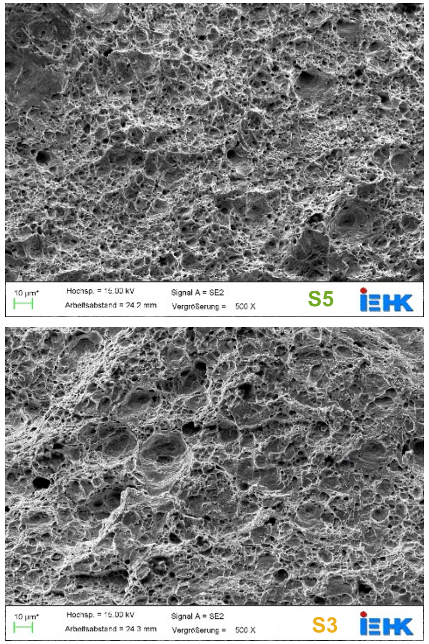

$$\bar{\varepsilon}_{df} = \left[\left(D_1^{df} \cdot e^{-D_2^{df}\cdot\eta_{avg}} - D_3^{df} \cdot e^{-D_4^{df}\cdot\eta_{avg}}\right)\bar{\theta}_{avg}^2 + D_3^{df} \cdot e^{-D_4^{df}\cdot\eta_{avg}}\right] \cdot f_{df}\,(C_{H^+})$$

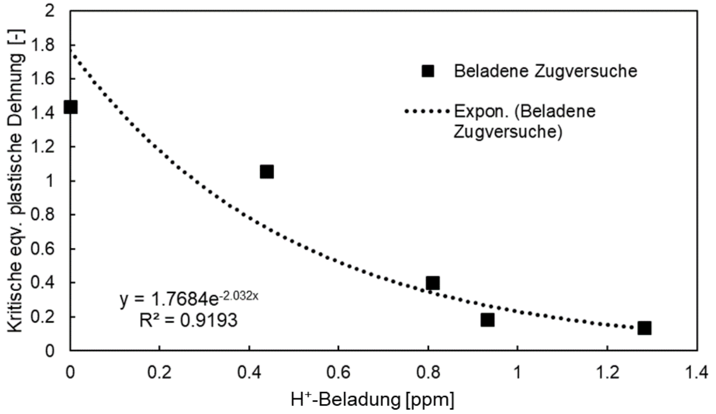

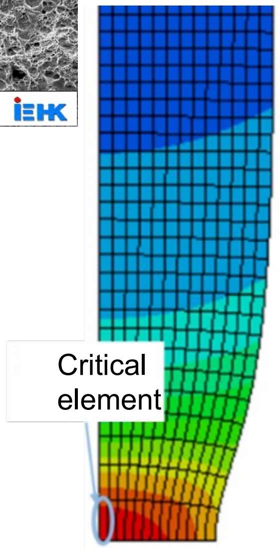

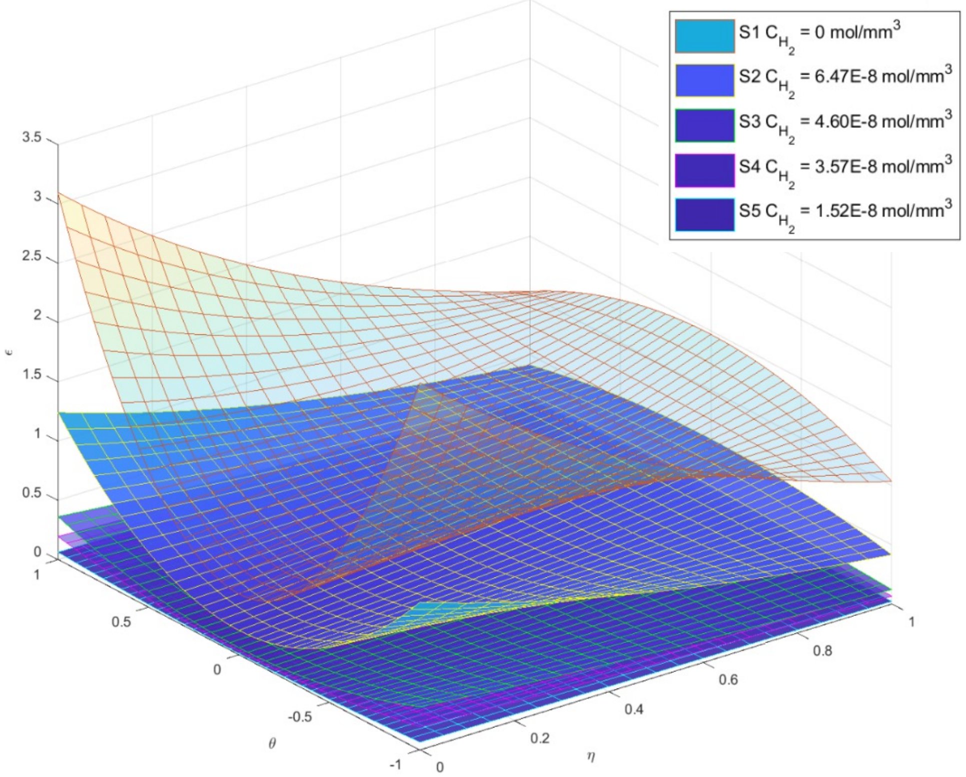

Step 1:
3D Pipe forming simulation on macroscale

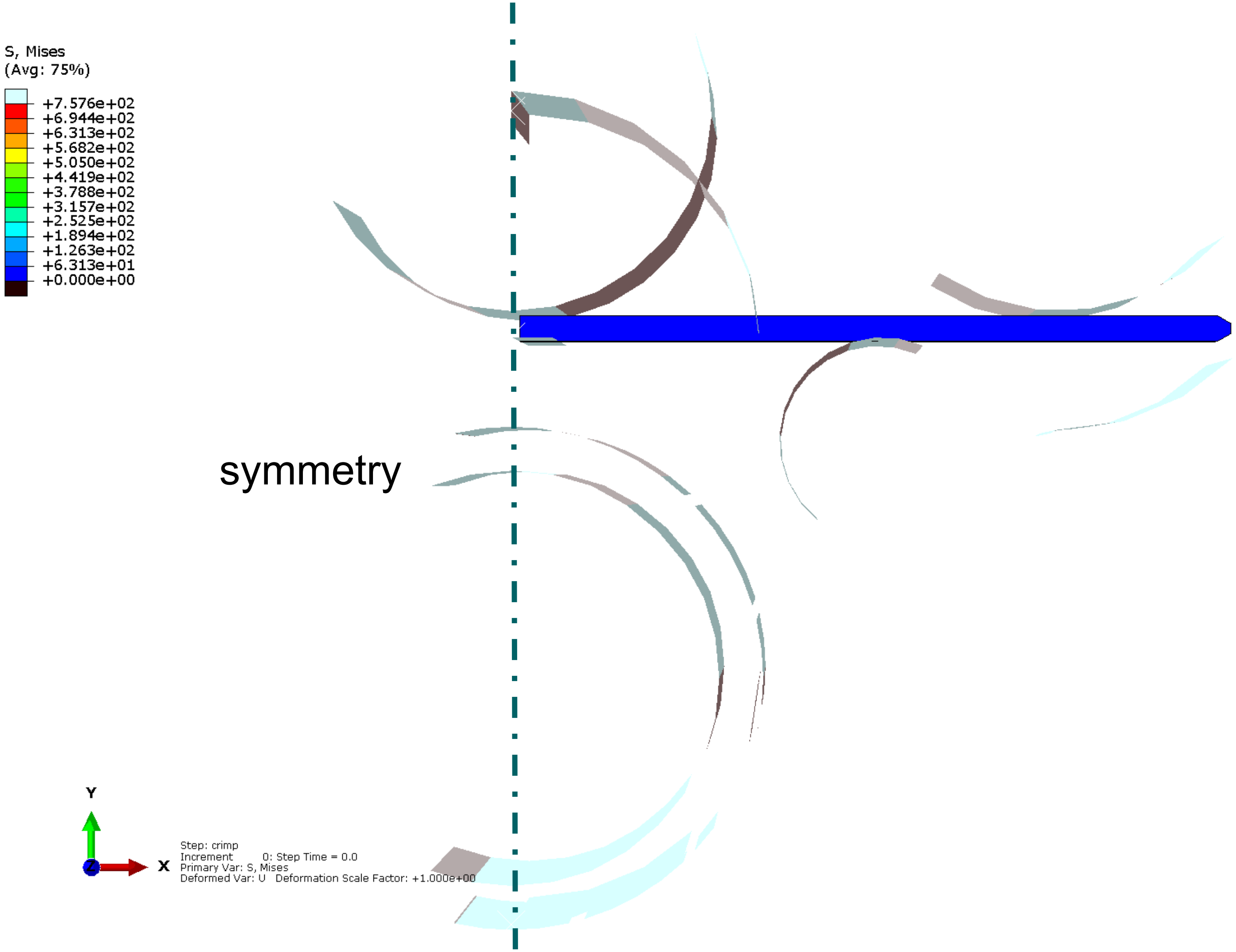

3D Pipe forming simulation on microscale

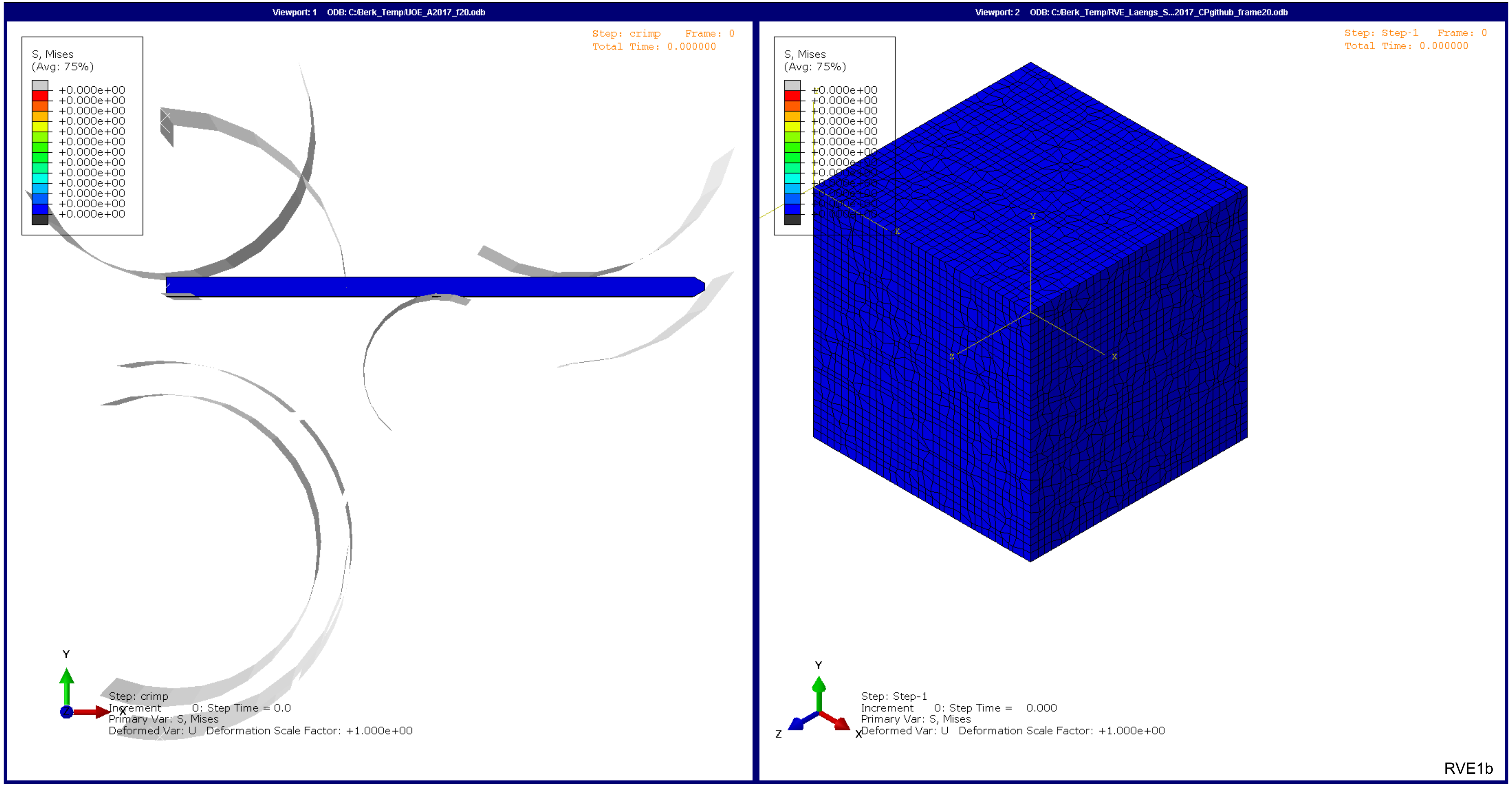

Sim. of hydrogen diffusion on the microscale based on UOE deformation history

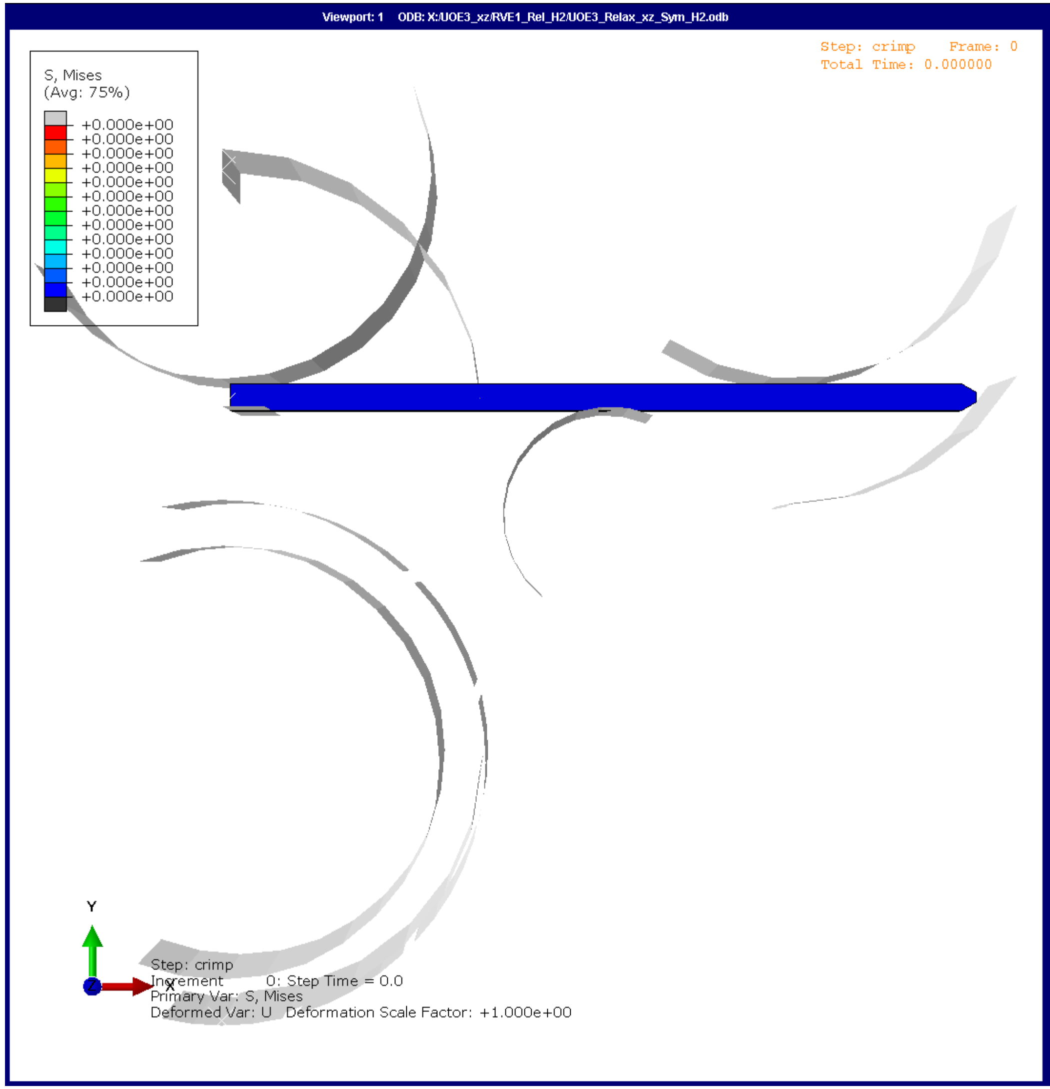

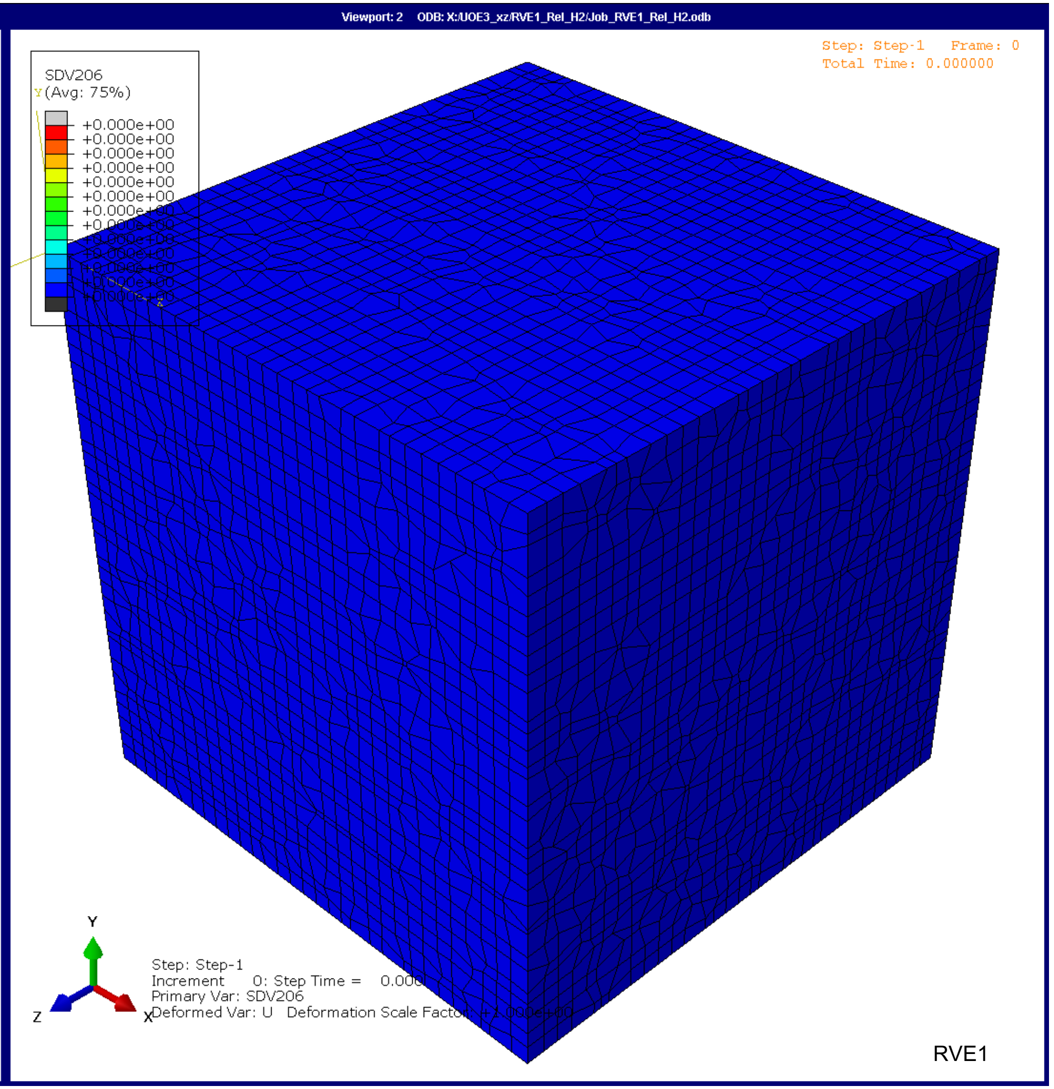

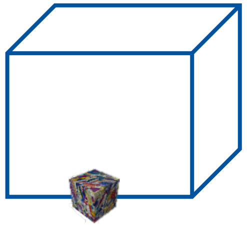

$$\bar{C}_{L,0} = 3{,}75x10^{-8}$$
mol/mm^3

Conclusions

- New structure at IBF with two chairs
- Continuation of existing research topics + exploration of new topics
- New topics: Multiscale modelling of microstructure evolution along the process chain including component performance evaluation
- A stronger focus on „non-steel topics“ is desired for the new chair of material modelling in forming technology
- Application examples show the research projects address relevant open questions
- For questions: sebastian.muenstermann@ibf.rwth-aachen.de

Thank you very much for your attention!